Science of the Total Environment 790 (2021) 148211

Contents lists available at ScienceDirect

Science of the Total Environment

journal homepage: www.elsevier.com/locate/scitotenv

Metal-Organic Frameworks (MOFs) as methane adsorbents: From storage to diluted coal mining streams concentration

David Ursueguía, Eva Díaz, Salvador Ordóñez *

Catalysis, Reactors and Control Research Group (CRC), Department of Chemical and Environmental Engineering, University of Oviedo, Julián Clavería s/n, 33006 Oviedo, Spain

HIGHLIGHTS

- Ventilation Air Methane (VAM) is emitted in low concentration 0.1–1%.
- CH_4 capture could generate an additional energy source or a chemical feedstock.
- Temperature swing adsorption with MOFs as adsorbents could separate the methane.
- Specific surface area and open metal sites are critical features for MOFs.
- Engineering aspects (shaping, pressure drop) are still challenging.

GRAPHICAL ABSTRACT

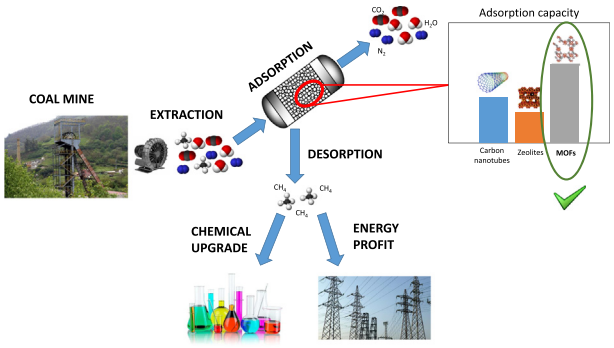

ARTICLE INFO

Article history:
Received 2 May 2021
Received in revised form 29 May 2021
Accepted 29 May 2021
Available online 4 June 2021

Editor: Huu Hao Ngo

Keywords:
Methane
Mining
Selectivity
MOF
Adsorption
Separation

ABSTRACT

Ventilation Air Methane emissions (VAM) from coal mines lead to environmental concern because their high global warming potential and the loss of methane resources. VAM upgrading requires pre-concentration processes dealing with high flow rates of very diluted streams (<1% methane). Therefore, methane separation and concentration is technically challenging and has important environmental and safety concerns. Among the alternatives, adsorption on Metal-Organic Frameworks (MOFs) could be an interesting option to methane selective separation, due to its tuneable character and outstanding physical properties.

Most of the works devoted to the methane adsorption on MOFs deal with methane storage. Therefore, these works were reviewed to determine the properties governing methane-MOF interactions. In addition, the metallic ions and organic linkers roles have been identified. With these premises, decisive effects in the methane adsorption selectivity in nitrogen/methane lean mixtures have been discussed, since nitrogen is the most concentrated gas in the VAM stream, and it is very similar to methane molecule.

In order to fulfill this overview, the effect of other aspects, such as the presence of polar compounds (moisture and carbon dioxide), was also considered. In addition, engineering considerations in the operation of fixed bed adsorption units and the main challenges associated to MOFs as adsorbents were also discussed.

Contents

* Corresponding author.
E-mail address: sordonez@uniovi.es (S. Ordóñez).

https://doi.org/10.1016/j.scitotenv.2021.148211

1. Adsorption processes for methane recovery

Methane fugitive emissions from coal mining constitute a significant contribution to greenhouse gases, even after exploitation closure (Pavloudakis et al., 2020; Gao et al., 2020). Typically, methane is emitted discontinuously through mining ventilation air in concentrations between 0.1 and 1% (Su et al., 2005). The flow rates of ventilation air methane (VAM) emissions vary from almost steady-state, through cycles that follow mineral production rates, to the hazardous phenomena of gas outburst or sudden large emissions (Szlazak et al., 2020). Around 70% of the worldwide methane emissions from underground coal mines consist of VAM from coal mine shafts (Borowski et al., 2020). In these emissions, methane concentration is fixed by safety constraints. The flammability limit for methane/air mixtures is between 5 and 15% of methane. Therefore, within the limits, methane could explode, being the explosion expanded in presence of combustible coal dust (Erdogan et al., 2014). In addition to the safety risks, the environmental concern is also remarkable since methane is a powerful greenhouse gas (GHG). Methane global warming potential (GWP) is about thirty times higher than that of carbon dioxide (Derwent, 2020). In this way, a study about the environmental impact of mining exploitations, using both carbon and ecological footprint, demonstrated that the most important contribution to the environmental impact corresponds to the ventilation of the gases generated in the shafts (Díaz et al., 2012).

Despite its importance, the removal of methane from VAM is still a technological challenge. The most common practice is the combustion of exhaust mining emissions (Shah et al., 2015; Qin et al., 2016). However, this technique has two important drawbacks, the requirement of auxiliary fuel, and the low energy efficiency. In order to overcome those drawbacks, it is possible either to implement catalytic combustion or regenerative catalytic oxidation (RCO). The first has low energy consumption and insignificant formation of noxious by-products such as thermal NO_x (Niu et al., 2019a). In the second case, the feed flow direction is periodically reversed, achieving an autothermal operation (Li et al., 2017). Another possibility is to capture and utilize the stream, generating an additional energy source (Oboirien et al., 2018; Singh and Kumar, 2016), with better yields for higher methane concentration in a rotary kiln or in a gas turbine combustion, or a chemical feedstockfor ethylene or methanol manufacture through catalytic reactions (Xie et al., 2018; Álvarez et al., 2020). Due to the mentioned intrinsic features of these streams, diluted gases in large flows with important variations of concentration (Yin et al., 2020; Cluff et al., 2015; Zheng et al., 2015; Baris, 2013), a previous concentration step is required (Karakurt et al., 2011). The removal of nitrogen, carbon dioxide, oxygen and water from the main stream is needed to effectively concentrate the methane of these emissions (Goraya et al., 2019). The challenge is to separate methane (<1%) from a mixture of mainly nitrogen (78.1%) and oxygen (20.9%), combined with high relative values of humidity and traces of carbon dioxide (near 0.1%), at ambient temperature and pressure with flowrates of even 45 m^3/s (Fernández et al., 2016; Su et al., 2008).

In general, the most important techniques for these separations are absorption, membrane separation and adsorption. Absorption is a mass transfer operation that uses specific solvents with different absorption capacities for different gas molecules. This operation is usually employed in the removal of impurities, instead of in the concentration of a minority compound. For example, natural gas sweetening, in which adsorbents such as di-ethylene (DE) or tri-ethylene (TE) glycol dimethyl ethers selectively remove carbon dioxide from the main stream (Henni et al., 2006). Regarding membrane separation, the simplest purification way is to let selectively the methane pass through. Satisfactory results have been achieved by this technique for both carbon dioxide and nitrogen separations from methane (Anderson et al., 2012; Lokhandwala et al., 2010). However, one of the most important limitations of membrane technology is the scaling up of its modules, since the pressure drop, and the module risk of damage are directly related to its size (Koc et al., 2013). Therefore, the large-scale manufacturing of selective membranes is still not technologically mature (Mi, 2019). Concerning the third proposed option, adsorption is one of the major technologies that is promising for increasing methane concentration in exhaust ventilation conducts, Fig. 1. This technique can achieve the minimum methane required to operate, e.g., in a gas turbine. In fact, Saleman et al. (2015) reached enrichments up to 51.3% of methane from streams containing initially 2.4% of methane.

The typical adsorption equipment consists of a column packed with an adsorbent material. At the adsorption stage, it is obtained a stream enriched in the most weakly retained component. In this case, methane is supposed to be one of the most strongly adsorbed components, so subsequent desorption allows obtaining a methane enriched stream Fig. 2. Occasionally, other individual separations of vapours and gases (water, carbon dioxide, etc.) or particles (to avoid erosion, adsorbent fouling, compressor damage and explosion risk) should be previously implemented (Su et al., 2008). The most common possibilities for adsorption/desorption processes at large scale are the swing adsorption methods. These processes use a cyclic variation of temperature (temperature swing adsorption, TSA) or pressure (pressure swing

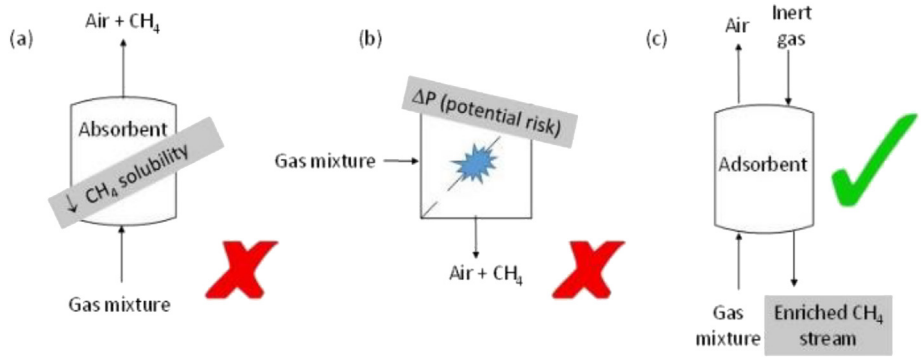

Fig. 1. Simple methane enrichment technologies selection: a) absorption, b) membrane separation and c) adsorption.

adsorption, PSA), alternating operation conditions between two or more available beds. In TSA processes, desorption is performed by increasing the temperature of the gas stream during the regeneration. On the other hand, PSA cycles are carried out either by lowering the partial pressures of the adsorbates or by reducing the total pressure by flowing a portion of the product gas over the adsorbent (Li et al., 2009). Usually, for gas purification processes in which the concentration of the component of the gas stream to be removed is lower than 2%, TSA is recommended (Yang, 2003; Ghoshal et al., 2002).

To reach its scope, the adsorption process profits the different affinities of the multicomponent gaseous mixture components and the adsorbent. Therefore, selected adsorbent materials are a key parameter in the adsorption process. In fact, the main features of the adsorbents can greatly influence the yield of the process both at large and small scale. Among the different available adsorbent materials, inorganic molecular sieves and carbonaceous materials are the most common, being reported several experiences of methane storage and separation from other gases on these adsorbents (Kacem et al., 2015; Delgado et al., 2007; Cavenati et al., 2004). In this way, Kim et al. (2013) have published a comprehensive manuscript about methane separation from diluted and medium-concentrated sources on these materials. Concerning the inorganic materials, the authors have researched experimentally 190 samples and over 87,000 simulations ordered by crystallographic structures, with the aim of looking for a material with adequate structural characteristics for the methane separation [37]. For these materials, adsorption and selectivity are usually characterized by steric effects, depending on the size of the adsorbate molecule and the pore, and also by the cationic nature of the surface (Gholipour and Mofarahi, 2016). In general, adsorbate molecules with high quadrupole moments are preferentially adsorbed if they fit in structural pores. Hence, for methane separations from mixtures with low methane and carbon dioxide concentrations in nitrogen ($CH_4/CO_2/N_2 = 1/1/98$), scarce structures were identified with CH_4/CO_2 separation ratios of 1.5 onwards. Therefore, inorganic materials are not optimal for methane separation from carbon dioxide, since the strong interaction of carbon dioxide molecule on the structural cations leads to poor selectivity values. In addition, similarities between molecular size of methane and nitrogen difficult to separate them through typical steric effects (Ghazvini et al., 2021). Further, methane adsorption capabilities are rather low (Kim et al., 2013; Javani et al., 2020). On the other hand, carbonaceous materials have also shown low CH_4/N_2 selectivities for different kinds of coal-based activated carbons, in addition to poor total adsorption capacity results (Yi et al., 2013; Yuan et al., 2018; Zheng et al., 2019). In general, the adsorption capacity of these materials depends on the accessibility of the adsorbate to the porous structure, due to their large specific surface area (Hou et al., 2020). These materials have shown larger adsorption capacity for carbon dioxide than for nitrogen, methane and oxygen (Esteves et al., 2008; Carrott et al., 2006). The higher polarizability of CO_2 promotes its adsorption. Then, some additional difficulties in the implementation of these materials for the methane separation could appear. These are mainly related to their fixed structure, porosity and specific surface area of inorganic molecular sieves and carbonaceous materials (Lin et al., 2017).

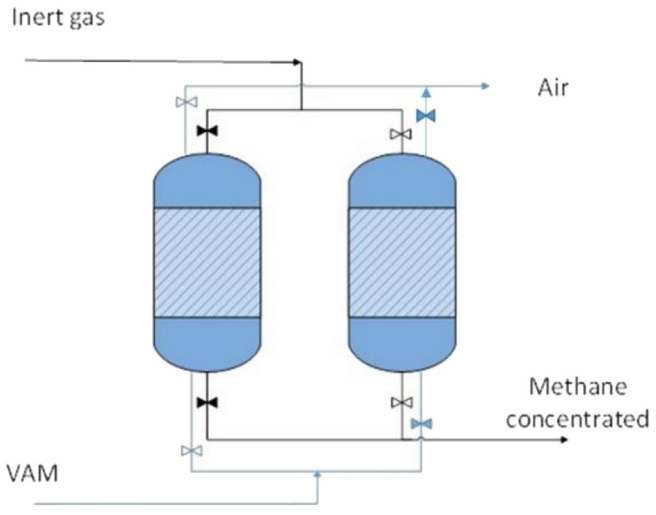

Fig. 2. Schematic figure of an adsorption unit. Alternatively, one bed is in adsorption (grey line), whereas the other one is in regeneration mode (black line).

Therefore, the usual adsorbents present serious limitations in low-concentrated methane adsorption and concentration. These materials show low methane adsorption capacity compared to carbon dioxide, and a very similar adsorption capacity compared to nitrogen. In addition, selectivity is mainly based on the molecular size differences, which in case of methane and nitrogen is very low. In fact, many of these materials require structural modifications for improving their performance, which would greatly make the process more expensive (Zhang et al., 2018; Wang and Yang, 2019). Due to these limitations, the use of the materials known as Metal-Organic Frameworks (MOFs) has emerged as an alternative for overcoming the previous problems. The interest in these materials was initially focused on developing gas storage systems for different purposes, such as hydrogen storage for automotive applications or carbon dioxide capture due to concerns over greenhouse emissions (Sridhar and Kaisare, 2020). In the case of the methane, as alternative to compressed natural gas, it consists of gas storing as and adsorbed phase in a porous solid (Düren et al., 2004). These materials are constituted by two main building blocks: a metal ion or metal oxide and an organic linker. The structures formed by these materials are diverse, since many different combinations of metallic ions and the organic linkers can be made. In addition, the variety of linker molecules, which may be functionalized to introduce changes directly into the framework, offers the possibility of turning the host/guest interactions and tailoring the materials rationally for a determinate separation (Düren et al., 2004; Ghanbari et al., 2020). A vast

number of works have related the surface area, pore size, adsorption heat, open metal sites and ligand functionalization with methane storage performance (Zhou, 2010; Wu et al., 2009). Consequently, finding the most effective features of MOFs for the storage and separation of methane from diluted streams can be a turning point in the methane emissions recovery process.

MOFs are then considered as an interesting alternative for methane concentration from VAM emissions. In order to explore this possibility, we will firstly discuss the mechanism of the methane adsorption on these materials (using available data in methane storage). The characteristics of the best materials will be described by families, in order to determine the most suitable features for the adsorption of methane. After this, the selectivity for methane adsorption in inert mixtures will be studied, determining those factors limiting the adsorption performance in gas mixtures. Finally, the effect of other reactive gases (such as humidity or CO_2) in the MOF performance and stability will be discussed. In the last part of the review, we will focus on the engineering aspects linked to the use of MOFs as methane adsorbent in practical applications. Aspects as pressure drop or adsorbent conformation, very scarcely treated in the open literature, will be considered at this point.

2. Adsorption of pure methane on MOF materials: insights from methane storage

Adsorption is an equilibrium-limited process, in which the different physical and chemical interactions between the adsorbent and the gas stream components allow the gas separation or storage (Yang, 2003). Therefore, in addition to convenient mechanical properties, both methane total adsorption capacity and its selective adsorption are decisive in the adsorbent material selection. Besides, favourable adsorption kinetics and high regenerability are desirable properties. These properties are usually related to the specific surface area, pore size, material composition and the existence of preferential active sites for adsorption, in addition to the surface characteristic polarity (Li et al., 2009).

From the point of view of methane-MOF interaction, MOFs present two main sites for methane adsorption: 1) coordinatively unsaturated metal ions (CUS), also called open metal sites (OMS), in which methane binds directly with the metallic ions of the structure through an electrostatic interaction, and 2) enhanced Van der Waals (VdW) potential pockets, in which there is a much weaker interaction, mainly related to the pore size (Zhou, 2010). These features lead to adsorption capacities largely higher than the corresponding to carbonaceous materials and zeolites, being this difference more marked at mild conditions (Rother and Fieback, 2013). The adsorption isotherms of MOFs usually follow a type I trend, reaching saturation at high pressures. Dietzel et al. (2009) presented the adsorption isotherms for different MOFs and adsorbates, evidencing the existence of these two main adsorption sites. Moreover, it is observed a decrease of the adsorption isosteric heat once the open metal sites are fully saturated with methane. In this way, Wu et al. (2010)) have described the two adsorption sites in the structure of different MOFs for methane adsorption (Fig. 3).

In recent years, many experiments and molecular simulations have dealt with methane and natural gas storage in MOFs. The main objective is to achieve a high density of methane at charge pressure, and be almost completely released at discharge pressure, thus boosting the working capacity. Computational screening has enabled the study of thousands of MOFs and suggested the existence of a physical limitation on methane storage with a maximum working capacity of 200 cm^3 (STP) cm^{-3} (Li et al., 2016a). Most of these experiments were developed at high pressures, with the uptake measured by two methods: 1) gravimetric, with a microbalance recording the change in weight of a sample at different methane pressures, and 2) volumetric, with a Sievert's equipment measuring the pressure change when dosing methane into a cell filled with the adsorbent [59]. In Table 1, a compilation of MOFs is classified at intervals of pressure by total methane adsorption capacity. For each one, information about their physical features, such as specific surface area or open metal sites presence, as well as the mechanism of methane adsorption, is collected. Subsequently, it is carried out a family classification. Some of these features along with the adsorption capacity will be very useful for selecting the best materials for the gas separation process. The vast number of materials tested at pressures equal or lower than 35 bar is due to that pressure is the maximum achievable by a one-step compressor (Ramos-Fernández, 2014). Therefore, a large number of experiments were performed to further extrapolation to higher pressures, trying to meet more easily DOE's objective: 350 cm^3 (STP) cm^{-3} (Li et al., 2016b). In addition, it is possible to observe great discrepancies among adsorption capacities obtained for the same materials and at similar conditions. At this point, it is important to remark that both experimental, by different techniques, and simulated values are included. Likewise, Chowdhury et al. (2009) pointed out that impurities or defects on the crystalline structure of MOFs could be responsible of large differences in the adsorption behaviour, being the point especially relevant since most of the reported MOFs have been synthetized at small scale in the laboratory.

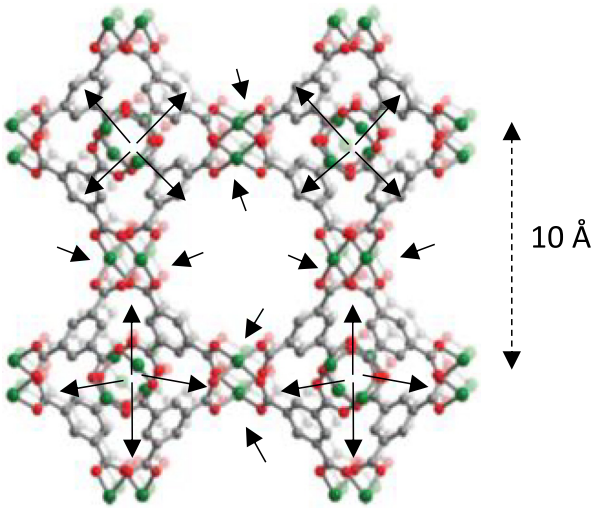

Fig. 3. Distribution of methane adsorbed onto HKUST-1 structure (Mason et al., 2014). The arrows point towards the higher mass methane load in the structure.

2.1. DUT MOFs

Four DUT (Dresden University of Technology) MOFs were presented for methane adsorption at 298 K and different pressures. DUT-49, the material with the highest methane adsorption capacity, is formed by a carbazole derived and metallic ions of copper (Stoeck et al., 2012). This material is an example of a pressure-amplifying material (Fig. 4), which enhances methane adsorption capacity at high pressures (Krause et al., 2018; Polyukhov et al., 2020). It presents a BET specific surface area of 5480 m^2/g and a total pore volume of 2.91 cm^3/g (Zhang et al., 2020). DUT-6, formed by metallic ions of zinc, presents a high methane adsorption capacity at 100 bar. Its high methane adsorption capacity at high pressures is attributed to its mesoporous character, combined with a high BET specific surface area of 2874 m^2/g and a total pore volume of 2.02 cm^3/g (Gedrich et al., 2010; Sahoo, 2016).

DUT-9 is formed by benzene-1,3,5-tribenzoate linkers and nickel clusters. It has a BET specific surface area of 3400 m^2/g and two different pore sizes (13 and 25 Å) (Gedrich et al., 2010). It presents a remarkable methane adsorption capacity of 203 mg/g at 35 bar, which is attributed to its high specific surface area and the presence of open metal sites in its structure. In contrast, DUT-52, formed by the link of 2,6-naphtalenedicarboxylate and metallic ions of zinc, presents a poor total methane adsorption capacity at 40 bar, which is related to its low BET specific surface area (1399 m^2/g) and accessibility, with a pore size of 8.6 Å (Krause et al., 2018). Therefore, these materials confirm

Table 1
Methane storage capacity at different pressures. Shaded areas facilitate the reading between pressures.

Adsorbent	Uptake (mg/g)	Pressure (bar)	Temperature (K)	Technique	Reference
Al-BTC	139.2	200	303	Volumetric	Knyazena et al. (2019)
DUT-49	308	110	298	Gravimetry	Bon (2017)
DUT-6	230	100	298	Volumetric	Gedrich et al. (2010)
MOF-177	221	100	298	Volumetric	Saha et al. (2010)
DUT-9	188	100	298	Gravimetry	Gedrich et al. (2010)
MOF-5	172	100	298	Volumetric	Saha et al. (2010)
Mg-MOF-74	120	100	298	Volumetric	Dietzel et al. (2009)
Ni-MOF-74	100	100	298	Volumetric	Dietzel et al. (2009)
MIL-101(Cr)	239	80	298	Volumetric	Llewellyn et al. (2008)
Al-soc-MOF-1	510	65	270	Simulation	Li et al. (2016a)
Al-soc-MOF-1	420	65	298	Volumetric	Alezi et al. (2015)
Al-soc-MOF-1	414	65	298	Simulation	Li et al. (2016a)
MOF-210	410	65	298	Simulation	Li et al. (2016a)
UTSA-76	263	65	298	Simulation	Li et al. (2014a)
MAF-38	246.4	65	298	Simulation	Li et al. (2018a)
HKUST-1	216	65	298	Simulation	Li et al. (2016a)
Ni-MOF-74	148	65	298	Simulation	Li et al. (2016a)
NU-111	320	60	298	Volumetric	Peng et al. (2013)
NU-125	250	60	298	Volumetric	Peng et al. (2013)
HKUST-1	200	60	298	Volumetric	Peng et al. (2013)
PCN-14	180	60	298	Volumetric	Peng et al. (2013)
UTSA-20	130	60	298	Volumetric	Peng et al. (2013)
Ni-MOF-74	110	60	298	Volumetric	Peng et al. (2013)
MIL-101(Cr)	122	50	303	Gravimetry	Wiersum et al. (2013)
MIL-125(Ti)	116	50	303	Gravimetry	Wiersum et al. (2013)
MIL-100(Fe)	104	50	303	Gravimetry	Wiersum et al. (2013)
UiO-66	80	50	303	Gravimetry	Wiersum et al. (2013)
MOF-177	170	40	298	Volumetric	Furukawa et al. (2010)
UiO-67	83.2	40	298	Simulation	Vandenbrande et al. (2017)
UiO-66	80	40	298	Simulation	Vandenbrande et al. (2017)
DUT-52	76.8	40	298	Simulation	Vandenbrande et al. (2017)
Mg-MOF-74	363	35	298	Volumetric	Alonso et al. (2017)
Ni-MOF-74	283.4	35	298	Volumetric	Alonso et al. (2017)
MOF-210	237	35	298	Volumetric	Mason et al. (2014)
DUT-9	203	35	298	Volumetric	Mason et al. (2014)
ZJU-5	200	35	298	Volumetric	Mason et al. (2014)
NJU-Bai10	199	35	290	Volumetric	Lu et al. (2013)
IRMOF-14	194	35	298	Simulation	Düren et al. (2004)
PCN-16	190	35	298	Volumetric	Mason et al. (2014)
IRMOF-14	186	35	298	Gravimetry	Senkovska and Kaskel (2008)
HKUST-1	183	35	298	Volumetric	Mason et al. (2014)
PCN-14	181	35	298	Volumetric	Wu et al. (2009)
Cu-tbo-MOF-5	175	35	298	Volumetric	Spanopoulos et al. (2016)
IRMOF-6	172	35	298	Gravimetry	Senkovska and Kaskel (2008)
IRMOF-6	171	35	298	Gravimetry	Ma and Zhou (2010)
IRMOF-1	165	35	298	Gravimetry	Spanopoulos et al. (2016)
PCN-11	163	35	298	Volumetric	Lovas et al. (2004)
IRMOF-993	160	35	298	Simulation	Wu et al. (2009)
Mg-MOF-74	158	35	298	Volumetric	Bao et al. (2011)
IRMOF-1	156	35	298	Simulation	Wu et al. (2009)
UTSA-20	155	35	298	Volumetric	Bao et al. (2011)
IRMOF-6	149	35	298	Simulation	Wu et al. (2009)
Cu-BTC	144	35	298	Gravimetry	Hamon et al. (2010)
Fe(bdp)	144	35	298	Volumetric	Mason et al. (2015)
Ni-MOF-74	138	35	298	Volumetric	Mason et al. (2014)
Co-MOF-74	135	35	298	Volumetric	Mason et al. (2014)
MOF-5	133	35	298	Volumetric	Wu et al. (2009)
HKUST-1	130	35	298	Volumetric	Zhou (2010)
Co(bdp)	128	35	298	Volumetric	Mason et al. (2015)
$Zn_2(BDC)_2(dabco)$	125	35	298	Volumetric	Hamon et al. (2010)
IRMOF-991	121	35	298	Simulation	Düren et al. (2004)
$Mg_2(dhtp)$	118	35	298	Volumetric	Wu et al. (2009)
MIL-53-Cr	114	35	304	Volumetric	Zhou (2010)
Ni-MOF-74	113	35	298	Volumetric	Zhou (2010)
$Ni_2(dhtp)$	113	35	298	Volumetric	Zhou (2010)
$CuSiF_6(4,4'\text{-byp})$	108	35	298	Gravimetry	Senkovska and Kaskel (2008)
$Co_2(dhtp)$	107	35	298	Volumetric	Wu et al. (2009)
$Mn_2(dhtp)$	105	35	298	Volumetric	Wu et al. (2009)
$Zn_2(dhtp)$	100	35	298	Volumetric	Hamon et al. (2010)
IRMOF-0	96	35	298	Simulation	Düren et al. (2004)
IRMOF-992	92	35	298	Simulation	Düren et al. (2004)
MOF-205	120	20	298	Simulation	Tahmooresi and Sabzi (2014)
MOF-177	100	20	298	Simulation	Tahmooresi and Sabzi (2014)
MIL-125(Ti)	84	20	303	Gravimetry	Wiersum et al. (2013)

(continued on next page)

Table 1 (*continued*)

Adsorbent	Uptake (mg/g)	Pressure (bar)	Temperature (K)	Technique	Reference
MOF-210	80	20	298	Simulation	Tahmooresi and Sabzi (2014)
MOF-200	80	20	298	Simulation	Tahmooresi and Sabzi (2014)
MOF-5	70	20	298	Simulation	Tahmooresi and Sabzi (2014)
Mg-MOF-74	93	10	298	Simulation	Becker et al. (2017)
Zn-MOF-74	77	10	298	Simulation	Becker et al. (2017)
Co-MOF-74	64	10	298	Simulation	Becker et al. (2017)
Ni-MOF-74	64	10	298	Simulation	Becker et al. (2017)
Ni-MOF-74	60	4	298	Volumetric	Dietzel et al. (2009)
Mg-MOF-74	50	4	298	Volumetric	Dietzel et al. (2009)
Basolite F300	110	1	130	Gravimetry	Sun et al. (2014)
HKUST-1	30.4	1	298	Volumetric	Wu et al. (2015)
Mg-MOF-74	28.8	1	278	Volumetric	Deng (2011)
Ni-MOF-74	20.4	1	298	Gravimetry	Li et al. (2014b)
Mg-MOF-74	17.6	1	298	Volumetric	Deng (2011)
HKUST-1	16	1	278	Volumetric	Wu et al. (2014)
Mg-MOF-74	16	1	298	Volumetric	Deng (2011)
HKUST-1	14.4	1	288	Volumetric	García et al. (2016)
HKUST-1	12	1	278	Volumetric	Wu et al. (2014)
HKUST-1	11.2	1	298	Volumetric	García et al. (2016)
MIL-53	11.2	1	278	Volumetric	García et al. (2016)
MIL-53	9.6	1	288	Volumetric	García et al. (2016)
Mg-MOF-74	9.6	1	318	Volumetric	Deng (2011)
MOF-177	9	1	298	Volumetric	Saha et al. (2010)
UTSA-16/GO	8	1	296	Volumetric	Szczęśniak et al. (2018)
HKUST-1	6.4	1	323	Volumetric	García et al. (2016)
MIL-53	6.4	1	298	Volumetric	García et al. (2016)
ZIF-8	6.4	1	278	Volumetric	García et al. (2016)
ZIF-8	4.8	1	288	Volumetric	García et al. (2016)
Fe(bdp)	4.8	1	273	Volumetric	Mason et al. (2015)
Fe(bdp)	4	1	285	Volumetric	Mason et al. (2015)
ZIF-90	3.5	1	303	Simulation	Phuong et al. (2016)
Fe(bdp)	3.2	1	298	Volumetric	Mason et al. (2015)
Co(bdp)	3.2	1	273	Volumetric	Mason et al. (2015)
MIL-53	3.2	1	323	Volumetric	García et al. (2016)
ZIF-8	3.2	1	278	Volumetric	García et al. (2016)
Co(bdp)	2.4	1	285	Volumetric	Mason et al. (2015)
MOF-5	2	1	298	Volumetric	Saha et al. (2010)
Co(bdp)	1.6	1	298	Volumetric	Mason et al. (2015)
ZIF-8	1.6	1	323	Volumetric	García et al. (2016)

that, at high pressures, high specific surface area materials and pore accessibility ensure the good behaviour as methane adsorbent.

2.2. Metal azolate frameworks (MAFs)

In this case, the same statement is applicable as for the DUT MOFs. MAF-38 is a metal azolate framework conformed by metallic zinc ions, and 4-(1H-pyrazol-4-yl)pyridine and 1,3,5-benzenetricarboxylic acid as organic ligands, Fig. 5. Although its methane adsorption capacity (246.4 mg/g) at 65 bar is considerable ($S_{BET} = 2229\ m^2/g$), it is in an intermediate position to MOF-210/UTSA-76 and Ni-MOF-74,

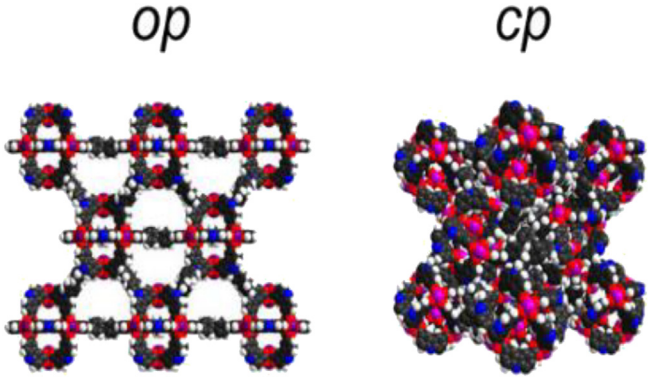

Fig. 4. Structure of DUT-49 in open and closed pore states: op and cp, respectively (Polyukhov et al., 2020). Cu, blue; O, red; C, grey.

characterized by its high density of open metal sites (Li et al., 2018a). Thus, its reduced pore sizes (6.2 and 8.6 Å) and total pore volume (0.808 cm^3/g) could reduce its adsorbent potential (Lin et al., 2016).

2.3. Zn_4O based MOFs

This group of MOFs is one of the most important, in terms of the number of materials, including the isoreticular metal-organic-frameworks (IRMOFs). The IRMOF structure is made of Zn_4O tetranuclear clusters connected by rigid dicarboxylic linkers to create a cubic framework, with square channels, which are connected in the three dimensions (Xiong et al., 2010; Wong-Foy et al., 2006), Fig. 6. MOF-210, with biphenyl-4,4′-dicarboxylate as organic linker, presents a BET specific surface area of 6240 m^2/g and a maximum pore size of 48.3 Å, with an aperture pore of 26.9 Å (Furukawa et al., 2010). This specific surface area is one of the largest surfaces ever reported for a crystalline material [73]. In addition, MOF-177 is formed by benzene-1,3,5-tribenzoate as organic linker, and presents a BET specific surface area of 4630 m^2/g, with a pore size of 12.7 Å (Saha and Deng, 2010a; Saha and Deng, 2010b). The great adsorption capacity of MOF-177 at 100 bar, 221 mg/g, remarks the role of surface area in methane storage at high pressures (Saha and Deng, 2010a).

Following the order of Table 1, IRMOF-14, with pyrene-2,7-dicarboxylate molecule as organic linker, presents one of the highest methane uptakes, attributed to its BET specific surface area of 4923 m^2/g and a pore size of 14.7 Å (Yang et al., 2012). IRMOF-6 and IRMOF-1, also called MOF-5, exhibit decreasing surface areas of 3025 m^2/g (Zhang et al., 2018; Vandenbrande et al., 2017) and 3100 m^2/g (Kaye et al., 2007), respectively, as well as decreasing pore volume, 9.1

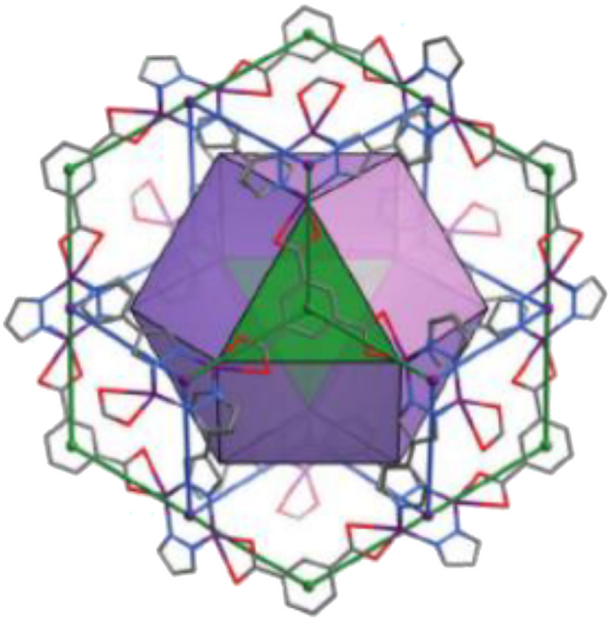

Fig. 5. Large quasi-cuboctahedral cage of MAF-38 (Lin et al., 2016). Zn, violet; C, grey; N, blue; O, red.

Å (Zhang et al., 2018; Vandenbrande et al., 2017) and 10 Å [104]. Additionally, Cu-tbo-MOF-5, a modification of IRMOF-1, was synthetized with the aim to improve methane storage (Spanopoulos et al., 2016), from 165 to 175 mg/g at 35 bar and 298 K. Also in this group, and with more reduced adsorption values, there are other materials that have in common its lower specific surface areas and reduced accessible pore diameters, conditioning in this way the methane uptake at these conditions. IRMOF-991, with ethinedicarboxylate as organic linker, presents a BET specific surface area of 3179 m^2/g and a pore size of 11.7 Å. IRMOF-993, with anthracene-9,10-dicarboxylate (ADC) as organic linker [105], presents a BET specific surface area of 1529 m^2/g and a pore size of 6.3 Å. This last material keeps a relevant methane uptake

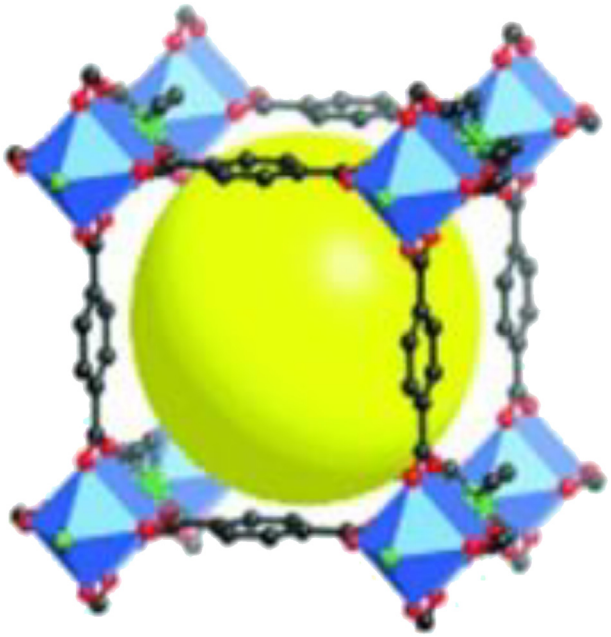

Fig. 6. Structure of IRMOF-1 (Kaye et al., 2007). The structure is common for the rest of the materials of the group.

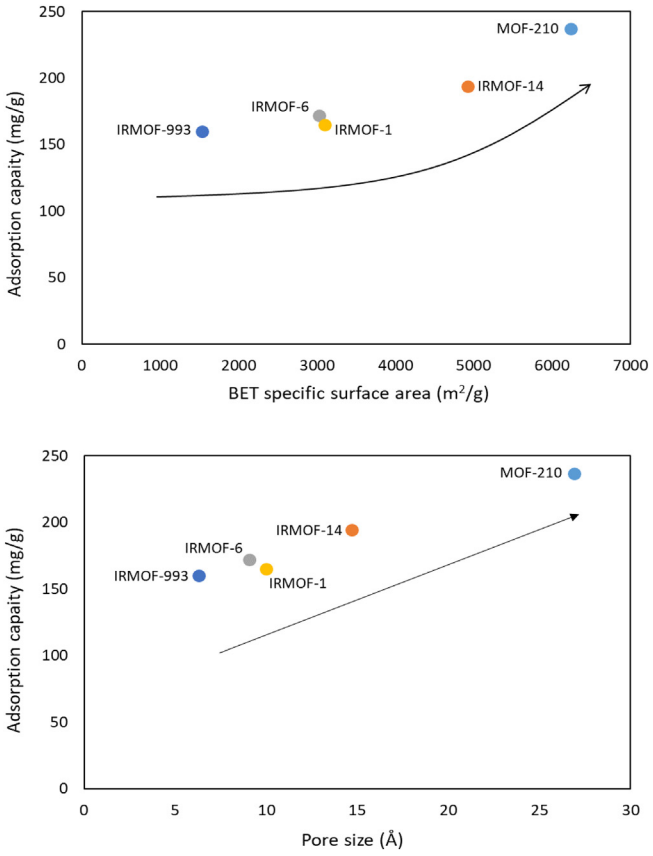

Fig. 7. Relationship between morphological properties and methane adsorption capacity at 35 bar for different MOFs.

due to the increment of the number of interaction sites and the reduction of the pore size near to the optimum value (Düren et al., 2004). Contrary, IRMOF-0, with a BET specific surface area of 1994 m^2/g and pore sizes of 8.5 and 9.7 Å and IRMOF-992, with 1381 m^2/g and 11 Å, respectively, have the poorest results [51], being attributed to the reduction of carbon atoms per cavity, which decrease the number of available active centers [51].

Fig. 7 shows a direct relationship between the morphological properties of Zn_4O based MOFs and their adsorption capacity at 35 bar. Consequently with previous discussions, at high pressures, methane total adsorption capacity increases with both specific surface area and pore size.

At 20 bar of pressure, most of the MOFs summarized in Table 1 belong to this group. As it is observed, methane adsorption capacity decreases significantly to values between 120 and 70 mg/g. MOF-205, with 2,6-naphtalenedicarboxylic acid as organic linker, exhibits a BET specific surface area of 4460 m^2/g and a pore size of 30 Å (Furukawa et al., 2010), what could be causing the highest adsorption capacity at these conditions. In the same way, MOF-200, formed by 4,4′,4″-(benzene-1,3,5-triyl-tris(ethyne-2,1-diyl)) tribenzoate as organic linker, presents a BET specific surface area of 4530 m^2/g and a pore size of 28 Å [73], with an adsorption capacity identical to MOF-210.

2.4. Square-octahedral (soc) based MOFs

MOFs based on the square-octahedral (soc) topology are expanded isoreticular structures (Alezi et al., 2015), and present the maximum capacities at 65 bar. Among them, Al-soc-MOF is formed by carboxyphenyl derived linkers and metallic ions of aluminium (Fig. 8). It has more than 2 cm^3/g of total pore volume and a BET specific surface area of 5585 m^2/g (Alezi et al., 2015; Wang et al., 2020). The structure encloses cubic-shaped cages of 14.3 Å, and exhibits either enhanced

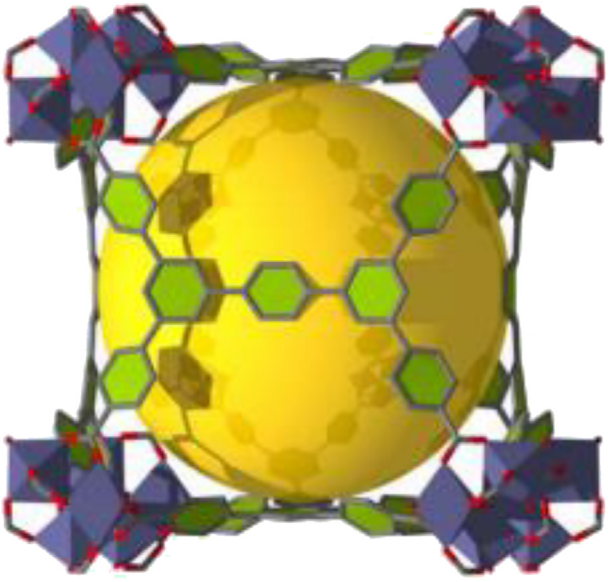

Fig. 8. Structure of Al-soc-MOF-1 (Alezi et al., 2015).

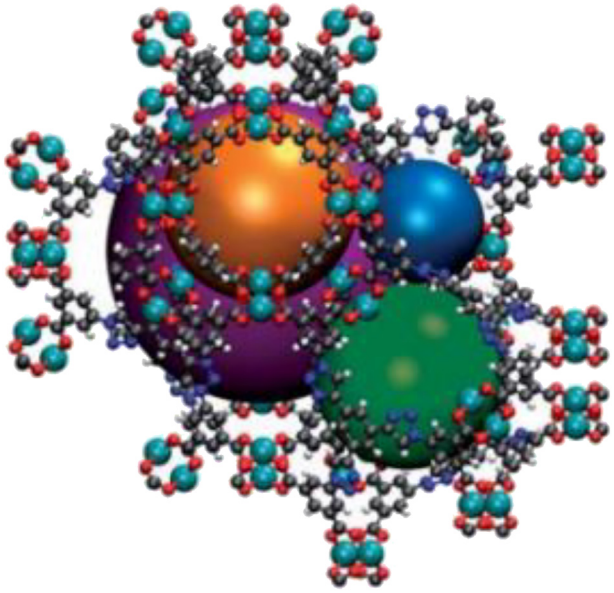

Fig. 9. Structure of NU-125 (Farha et al., 2012). C, grey; H, white; O, red; N, blue; Cu, cyan.

volumetric or gravimetric uptake equilibrium [68], with a strong influence of the temperature for constant pressures.

Alezi et al. (2015) aimed that this material exhibits a pore size near to the optimum for methane adsorption at high pressure. The same authors have done experiments maintaining the Al-soc-MOF platform, varying the MOF number (MOF-1,2,3). MOF-1 resulted the material with the highest BET specific surface area and the highest uptake capacity, surpassing at certain pressures DOE's objective. Therefore, the high capacity of this material at high pressures, even above other materials with a larger specific surface area, reveals that the total pore volume and the pore size are also very influential parameters in the adsorption.

2.5. NU-MOFs

The NU-MOFs (Northwestern University) series belong to rht-type-copper-hexacarboxylate frameworks. These materials arose from the search for greater adsorption capacity without compromising stability. NU-111 presents four different pore sizes (14, 17, 19 and 24 Å), which together with its large BET specific surface area (6140 m^2/g), make it an excellent adsorbent (Farha et al., 2012). Another NU-MOF, NU-125 (Fig. 9), formed by the link of hexacarboxylic acid and metallic ions of copper (Fig. 9), presents a BET specific surface area of 3105 m^2/g and good adsorption values at very low temperatures (Wilmer et al., 2013). These materials confirm the previously exposed theory, they are the best materials at 65 bar due to their high specific surface area. In addition, NU-111 presents about 50% more specific surface area than NU-125, which corresponds to an increase in methane adsorption capacity of 22% at 65 bar (Peng et al., 2013).

2.6. MIL-MOFs

MIL-MOFs (Materials Institute Lavoisier) are formed by terephtalic acid and different metallic ions with many possible combinations, Fig. 10. All the materials reported from this group presented similar uptake capacities despite its different structure. MIL-101(Cr) has a pore diameter of 16 Å and a BET specific surface area of 4000 m^2/g (Zhao et al., 2015). This material presents terminal water molecules connected to the octahedral trinuclear $Cr(III)_3O$ building units, creating potential Lewis acid sites, which conferees remarkable stability towards water (Hwang et al., 2008; Hong et al., 2009; Liu et al., 2013).

On the other hand, MIL-125(Ti) has titanium as metallic ions, a BET specific surface area of 1469 m^2/g and a minimum pore size of about 6 Å (Rahmani et al., 2018; Ramsahye et al., 2014). MIL-100(Fe) has iron as metallic ions, and a BET specific surface area of 1500 m^2/g (Tan et al., 2015). It presents two sets of mesoporous cages that are accessible through microporous windows of 5.5 and 8.6 Å (Dhakshinamoorthy et al., 2012). These results evidence the dominant role of surface area and pore volume in the methane adsorption capacity, as Lee et al. (2009) have demonstrated for these materials. The same authors remarked that MOFs should have high porosity for being applied as methane adsorbents.

2.7. UiO-MOFs

UiO-MOFs (Universitetet i Oslo) are made of $Zr_6O_4(OH)_4$ clusters. UiO-66 consists of a cubic framework with a BET specific surface area of 1100 m^2/g and pores of 10 and 7 Å. It is one of the adsorbents most widely used, due to its high chemical and thermal resistance (Ahmadijokani et al., 2020). UiO-67 presents biphenyl-4,4′-dicarboxylate organic linkers, a BET specific surface area of 2583 m^2/g and pores of 23 and 11.5 Å (Rahmani et al., 2018; Katz et al., 2013; Øien-Ødegaard et al., 2016). Similarly to MIL-MOF structures, UiO-MOFs present large octahedral and small tetrahedral pores (Fig. 11). Likewise, a significant amount of zirconium Lewis acid sites were observed on these materials (Ramsahye et al., 2014). These characteristics provide excellent thermal, chemical and mechanical stability to these structures.

Cavka et al. (2008) and Al-Jadir and Siperstein (2018) have studied the influence of the pore size and BET specific surface area on the performance of the UiO MOFs. It was observed that methane adsorption capacity is governed by the specific surface area, in agreement with previous observations at high pressures. In addition, it was concluded that the effect of the organic linker on macroscopic properties, such as pore size, is negligible at low pressures, becoming evident at higher ones.

2.8. M-MOF-74

These materials are formed by the link of 2,5-dihydroxyterephthalic acid as organic linker and different metallic ions. These MOFs exhibit a honeycomb-type structure in which the metal cations occupy the corners of hexagons formed by the organic linker (Fig. 12). The difference

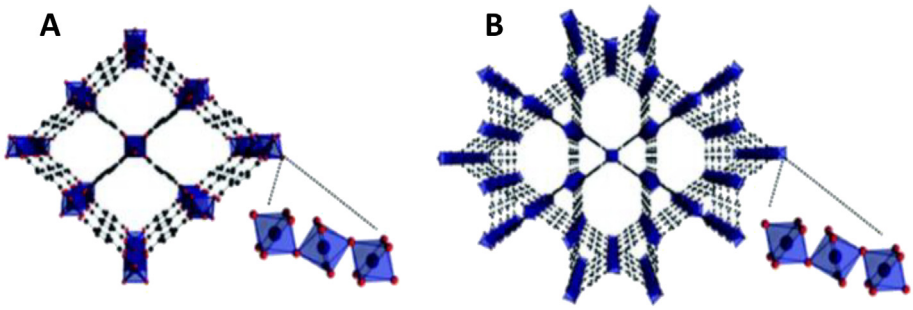

Fig. 10. Structure of MIL-MOFs (A: MIL-53(Al), B: MIL-68(Al)) (Embrechts et al., 2020).

in metallic ion (Mg, Ni, Zn, Mn, Co) can influence the morphology of the material, varying, e.g., from around 1500 m^2/g for Mg-MOF-74 to 500 m^2/g for Zn-MOF-74 (Glover et al., 2011). The pore size is about 11–12 Å, conditioning in this way their applications (Valvekens et al., 2014). In addition, the strength of the Lewis acid sites of MOF-74, arising from the presence of open metal sites, decreases in the order: Mg-MOF-74 > Ni-MOF-74 > Co-MOF-74 > Cu-MOF-74 (Cabello et al., 2016). This order is not the same in case of the concentration of open metal sites, which is between 2.9 and 3.4 mmol/g: Ni-MOF-74 > Co-MOF-74 > Mg-MOF-74 > Cu-MOF-74 [127]. Therefore, it is observed that, at low pressures, the concentration of open metal sites takes more importance than its strength, since Ni-MOF-74 presents higher methane adsorption capacity values than Mg-MOF-74. In addition, the presence of open metal sites provokes that the one-dimensional channels of the structure are easily filled with water, which can be removed by a mild thermal treatment (Bonino et al., 2008).

These results point out the strong impact of the metal site since the order in the adsorption capacity is not possible to be explained just by the morphology. For example, MIL-125(Ti), with a similar specific surface area than Mg-MOF-74, presents slightly lower adsorption capacity. Although the accessibility of MIL-125(Ti) is favoured, with a medium pore aperture of 69.8 Å versus to 11 to 12 Å for Mg-MOF-74, its higher strength and concentration of open metal sites make a difference (Cabello et al., 2016). Likewise, a decrease in the adsorption pressure from 10 to 4 bar just reduces in a 6% the methane uptake for Ni-MOF-74, whereas in case of Mg-MOF-74, this reduction value increases to 35%. Therefore, it is again demonstrated that the methane adsorption at reduced pressures is specially favoured by the concentration of open metal sites, instead of by its strength. In fact, open metal sites concentration at room temperature for Ni-MOF-74 is around 3.5 mmol/g for Ni-MOF-74, and 3 mmol/g for Mg-MOF-74 (Cabello et al., 2016; He et al., 2014).

2.9. PCN-MOFs

PCN-MOFs (Porous Coordination Network) is a sub-group formed by the link of different organic ligands and copper as metallic ions (Fig. 13). PCN-16 presents a NbO-type structure designated as the α-phase, a BET specific surface area of 2273 m^2/g and a pore size of 11 Å (Sun et al., 2010). On the other hand, PCN-14, with dinuclear $Cu_2(CO_2)_4$ addlewheel clusters, presents open metal sites that intensify the adsorption of gas molecules (Lucena et al., 2011). Copper metallic ions are linked by 5,5′-(9,10-anthracenedyil)diisophthalate (Mason et al., 2014). It has a BET specific surface area of 1984 m^2/g and a pore size of 8.3 Å. For a long time, it was one of the best materials for methane storage, so it was studied widely in several manuscripts (Peng et al., 2013; Ma et al., 2008). Finally, PCN-11 contains trans-stilbene-3,3′,5,5′-tetracarboxylate as organic linker. It has a BET specific surface area of 1931 m^2/g and a pore size of 12.5 Å [58]. These materials follow the same rule at high pressures as those discussed above. In this case, at 35 bar, the order of adsorption capacity is the same as the BET specific surface area.

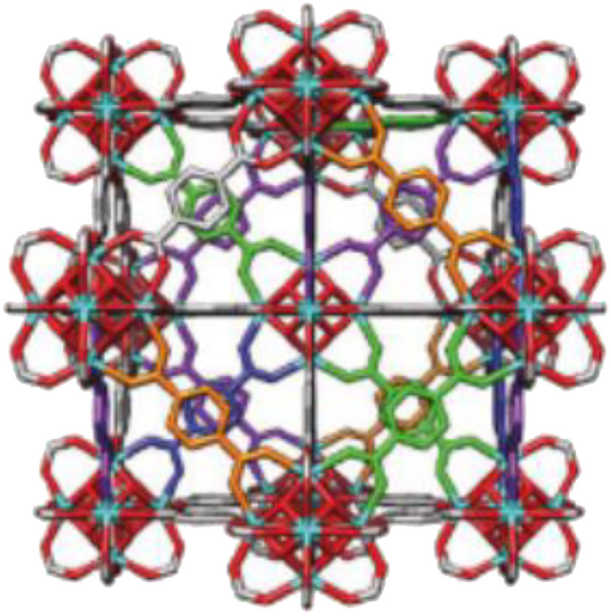

Fig. 11. Structure of UiO-66 (Lázaro et al., 2020). Zr, light blue.

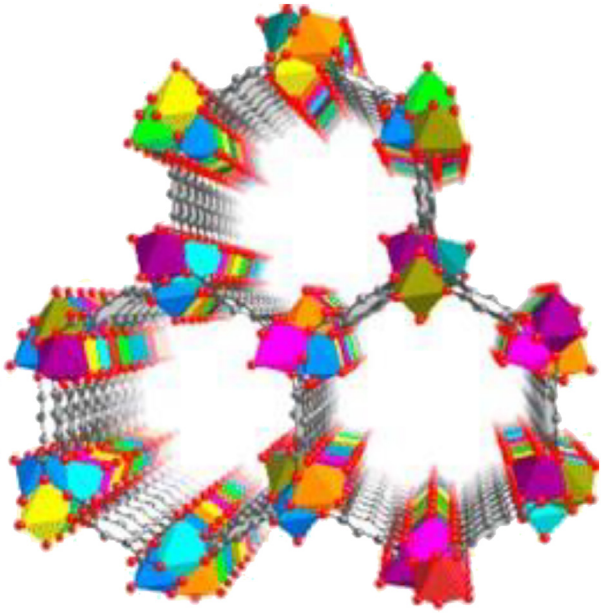

Fig. 12. Structure of M-MOF-74 (Wang et al., 2014).

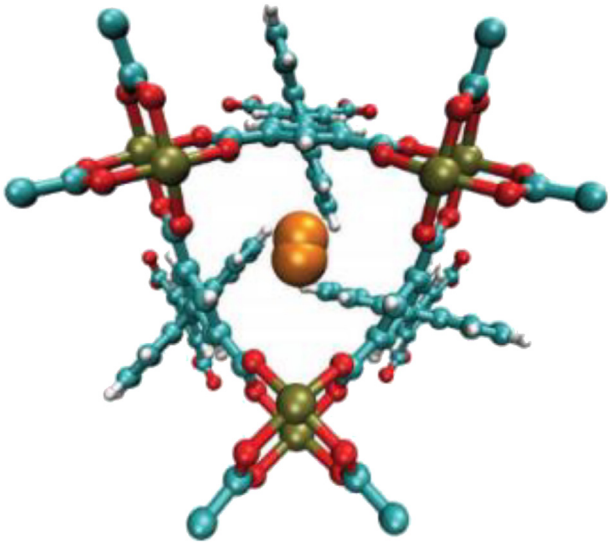

Fig. 13. Structure of PCN-14 (Pham et al., 2016). C, cyan; H, white; O, red; Cu, tan.

2.10. Basolite MOFs

Basolite is the commercial name of different adsorbent materials commercialized by BASF. Al-BTC, commercially available under the name Basolite A520, is formed by trimesic acid (1,3,5-benzenetricarboxylic acid) as organic linker and aluminium metallic ions. The structure presents a significant pore volume (0.59 cm^3/g) and a BET specific surface area of 1422 m^2/g, in addition to a large volume of mesopores of 50 Å (Knyazena et al., 2019). HKUST-1, also called Basolite C300, is formed by trimesic acid and copper metallic ions. It presents a BET specific surface area of 2100 m^2/g and a structure with small cages of 4, 10 and 11 Å (Peng et al., 2013). After removal of the axial water molecules typically linked to the structure, the copper atoms become coordinatively unsaturated for binding other gas molecules (Ghazvini et al., 2021). Only the cube-octahedral cage has open copper coordination sites into the pore (Fig. 14) (Kokçam et al., 2020). Similarly, Fe-BTC, also called Basolite F300, is formed by iron ions and trimesic acid. It has a BET specific surface area of 1600 m^2/g and a pore size of 21.7 Å (Dhakshinamoorthy et al., 2012), and presents available iron metal sites for methane adsorption. On the other hand, ZIF-8, also called Basolite Z1200, is a zinc-based material, with a BET specific surface area of 1947 m^2/g and a pore size of 3.4 Å (Park et al., 2006). As seen in the compilation, these materials follow the same previously described rule: the open metal sites enhance the adsorption capacity at low pressures, whereas the limited specific surface areas, in comparison to other MOFs, cause poor yields at high pressures. Likewise, ZIF-8, with narrow pore size of difficult accessibility, is one of the worst materials of the list.

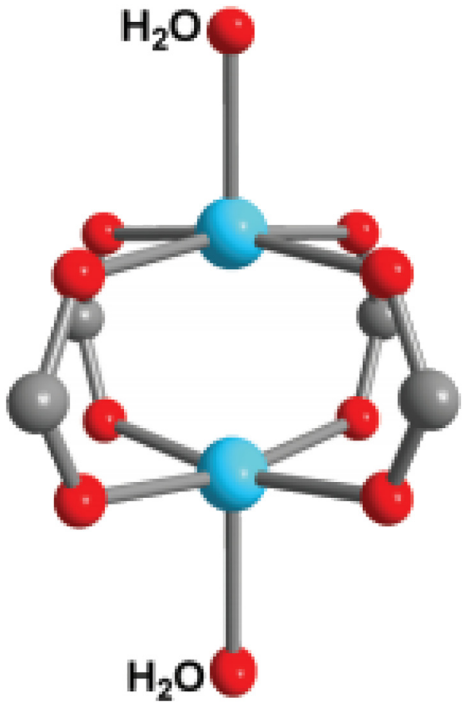

Fig. 14. Paddle-wheel unit of HKUST-1 (Kokçam et al., 2020).

2.11. UTSA MOFs

UTSA-20 (University of Texas San Antonio) is formed by triylhexabenzoic acid and metallic ions of copper. It presents a moderate BET specific surface area of 1150 m^2/g. The structure is formed by two different types of one-dimensional channels: one formed by rectangular pores (3.4 × 4.8 Å) and another cylindrical of 8.5 Å, with high density of open metal sites (Guo et al., 2011). On the other hand, UTSA-16, which is formed by the link of cobalt citrate and potassium ions, has a BET specific surface area of 687 m^2/g, and a pore size of 33 Å (Fig. 15). Its scarce surface available reduces considerably the methane uptake. However, it presents an impressive CO_2/CH_4 selectivity, with a ratio of 114.4 (Masala et al., 2016).

UTSA-76 is formed by metallic ions of copper and the semi-rigid organic linker H_4L. It presents a BET specific surface area of 2820 m^2/g and pore volume of 1.09 cm^3/g (Li et al., 2014a). In this case, despite the high density of open metal sites present in UTSA-20, at high pressures, the much larger specific surface area shown by UTSA-76 enhances the methane adsorption capacity.

2.12. Other MOFs

In addition to the families presented above, other MOFs have been included in Table 1. Two structures with copper as metallic ion present values of methane adsorption capacity, at 35 bar, around 200 mg/g, NJU-Bai10 (Nanjing University Bai's Group) and ZJU-5 (Zhejiang University), both also with pyridine-derived organic linkers. The former has a BET specific surface area of 2883 m^2/g, and three different pore sizes (11, 13 and 7 Å) (Lu et al., 2013). In addition, the latter has a BET specific surface area of 2823 m^2/g and it is characterized by its Lewis basic pyridyl sites and its suitable pore space (10.5 Å) (Rao et al., 2013). As seen, at high pressures, materials with similar BET specific surface area and pore size, present similar methane uptake capacities.

On the other hand, $CuSiF_6$(4,4′-byp) presents copper as metallic ion, and an adsorption capacity of around 100 mg/g at high pressures. Its lower adsorptive capacity can be attributed to the low BET specific surface area (1100 m^2/g) (Li et al., 2018a). Finally, concerning ZIF-90, it is a zinc based MOF. It possesses a BET specific surface area of 1270 m^2/g and a pore size of 3.5 Å (Nosike et al., 2020). Its low methane adsorption capacity may be due to its narrow pore size.

2.13. Other materials

Other materials were tested for methane adsorption, under similar conditions, with the aim of comparison. Following the pressure order, zeolite 5A has presented an uptake capacity of 144 mg/g at 100 bar and 298 K (Saha et al., 2010; Alonso et al., 2017), and 99.2 mg/g at 50 bar and 302 K (Wiersum et al., 2013). This material presents a pore size similar to the size of the methane molecule, which eases the adsorption process (Triebe et al., 1996). Here, it is pointed out a great

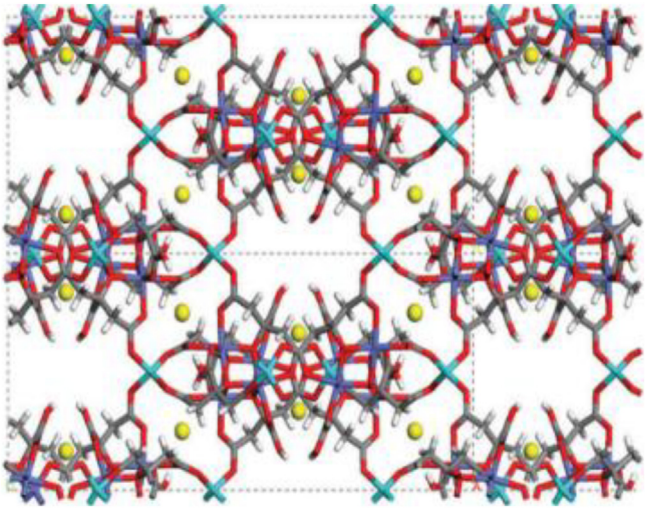

Fig. 15. Structure of UTSA-16 along x-axis (Masala et al., 2016). C, grey; H, white; O, red; Co, light blue for tetrahedral Co^{2+} and violet for octahedral Co^{2+}, K, yellow.

difference on the adsorption process between zeolites and MOFs. In the former, the adsorption could occur until filling the pore, whereas in the latter, it occurs a stronger interaction with metal centers combined with Van der Waals forces, or only Van der Waals forces in case of absence of open metal sites (Becker et al., 2017).

Kizzie et al. (2014), working with a porous polymer network (PPN), PPN-4, have observed an uptake of 150 mg/g at 50 bar and 298 K. The good properties of PPN: high adsorption capacity, low cost, ease of processing and high thermal stability (Lu et al., 2010), are just limited by the specificity of the interaction, which could limit their subsequent application for selective separations. Likewise, Alonso et al. (2017) raised the use of activated carbon, with an uptake of 224 mg/g at 47 bar and 298 K, whereas Wiersum et al. (2013) proposed the NaX zeolite, with an uptake of 56 mg/g at 40 bar and 303 K. Furukawa et al. (2010), in a compilation about covalent organic frameworks (COFs), organic linkers held together by boron oxide clusters by means of covalent bonds, offer very different adsorption capacities (Liu et al., 2010). In this way, COF-102, with an adsorption capacity of 187 mg/g at 35 bar and 298 K, presents the best performance. Likewise, mesoporous materials, such as MSM-41, have demonstrated poorer results at the same conditions: 41 mg/g (Wu et al., 2009).

2.14. Suitable features for methane adsorption

From the reviewed data, it is deduced that pure methane adsorption in MOFs upon 60 bar and 270 K is mainly proportional to the specific surface area and pore volume, whereas other features are less relevant. In the 40–60 bar range, the influence of the available surface area and pore volume is also significant, although the surface chemistry becomes more important. In the 30–40 bar interval, a change of the key factor is observed: add to the high surface area, the presence of open metal sites (main contributors to Lewis acidity), as well as metal atoms density within the cavity, contribute to enhance the methane uptake. This trend is more evident at atmospheric pressure. The positive influence of the concentration of active sites versus the strength of its interaction being also evident. In fact, the interaction strength decreases the adsorption capacity and hinders the subsequent desorption. Besides, the size of the cavities in which adsorption occurs and the size of the adsorbate molecule should be as close as possible, to increase the relevance of Van der Waals forces. Fig. 16 shows the influence of the surface area of the MOFs in the methane uptake. At atmospheric pressure, a clear

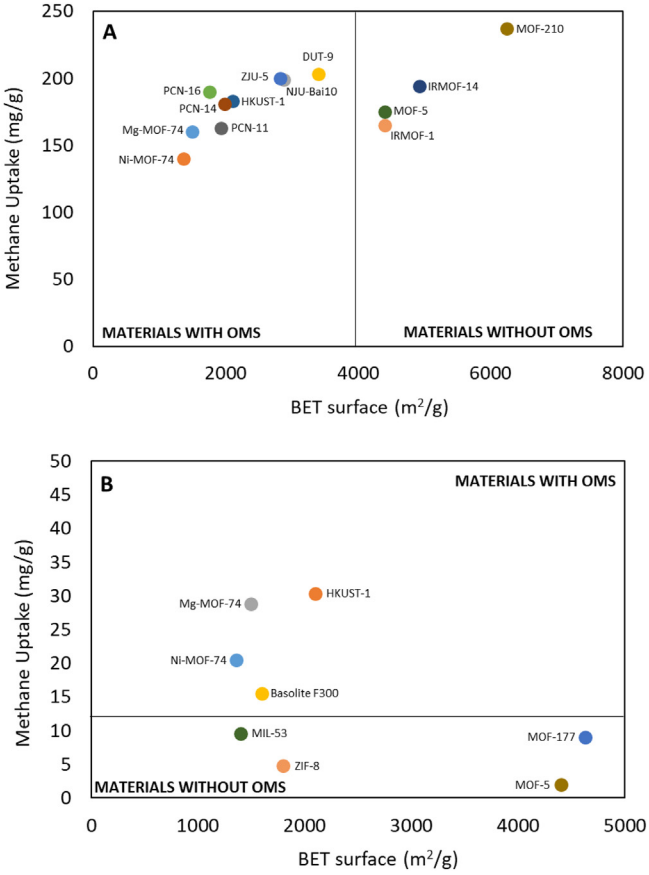

Fig. 16. Relation between methane uptake and BET specific surface area depending on the presence of open metal sites in the structure. **A**: 35 bar, **B**: 1 bar.

benefit of the presence of open metal sites is observed for methane adsorption, especially for MOF-74 and HKUST-1.

From the point of view of operation, in addition to a high adsorption capacity, it is desirable that the adsorbent is easily regenerable. In TSA configuration, where thermal regeneration occurs, it is convenient that low temperatures increments promote adsorbate desorption. At this point, Fig. 17 shows the appropriate behaviour of Mg-MOF-74, for which an increment of 20 K decreases in a 40% the methane storage. Its high concentration of open metal sites – instead of the strength – is determinant for the methane uptake and regeneration process. Similar reduction percentage (40%) is observed for the MIL-53 structure, but for a lower methane uptake value. In the case of HKUST-1, the material with the largest methane adsorption capacity at atmospheric pressure, the uptake reduction is around 30%. Therefore, here it is shown that the selection of adsorbent requires taking into account not only the adsorption capacity at the working conditions, but also the ease of regeneration.

3. Methane adsorption in gas mixtures

The scope of the previous section about pure methane adsorption was studying MOF properties determining methane adsorption performance: pure methane adsorption data provide information about the maximum adsorption capacity. However, diluted methane streams also require the study of selective adsorption from a multicomponent mixture (Tagliabue et al., 2009). In the case of VAM, methane separation from nitrogen is challenging because of the physicochemical similarities between methane and nitrogen molecules (Table 2). The dominant presence of nitrogen and the similar molecular radius with methane, require a separation based on the different affinities between both molecules to the adsorbent. Open metal sites act as the primary adsorption

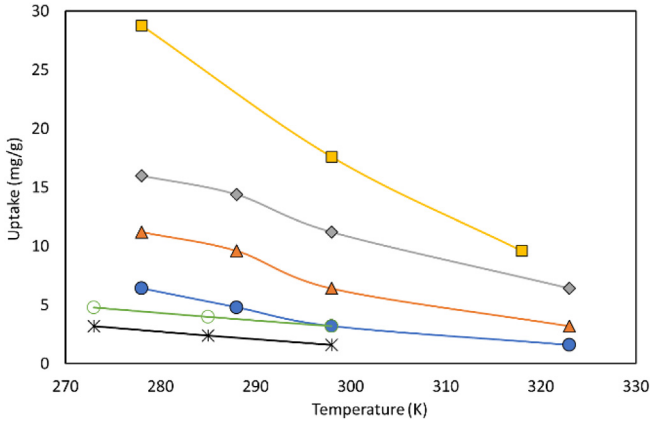

Fig. 17. Methane uptake profile with temperature for adsorption at 1 bar for different MOF structures. ZIF-8 (filled blue circles), MIL-53 (filled orange triangles), HKUST-1 (filled grey rhombus), Mg-MOF-74 (filled yellow squares), Co(bdp) (black flakes), Fe(bdp) (empty green circles).

site for methane. However, a strong interaction of adsorbate on these sites will avoid methane desorption, therefore, the work capacity will decrease while a higher desorption temperature will be required.

Similarly to the previous section, Table 3 summarizes the scarce works dealing with methane selective adsorption on MOFs from mixtures with nitrogen at low pressures. The first materials presented in Table 3 were either specifically synthesized for methane-nitrogen separations, or typical MOFs tailored with the same purpose. Al-CDC is formed by the link of trans-1,4-cyclohexanedicarboxylic acid and metallic ions of aluminium. It presents a BET specific surface area of 380 m^2/g and a pore size of 5.4 Å (Chang et al., 2020). The presence of a specific zone for methane adsorption in the structure increases the selectivity over nitrogen. In addition, the open metal sites promote the high adsorption capacity at low pressures even with a low specific surface area [148]. Li et al. (2018b) synthesized an ultramicroporous MOF with a BET specific surface area of 75.6 m^2/g and pore dimensions of 4.1 × 4.3 Å, $Co_3(C_4O_4)_2(OH)_2$. It is formed by enhanced negative oxygen binding sites, which add to high methane selectivity, it shows a low methane uptake.

In the structure, both molecules interact with the framework through multiple Van der Waals interactions, O↔H-C in case of methane and N↔O for nitrogen. The higher selectivity to methane is due to the more suitable pore size and the higher polarizability of the molecule (Li et al., 2018b). It is remarkable that the absence of important coulombic forces, due to the absence of open metallic sites, enhances the Van der Waals forces, which improves the separation efficiency, but decreases the total adsorption capacity.

Cu-MOF is a modification of the Basolite C300 (HKUST-1) with a distorted structure. This material presents a BET specific surface area of 110 m^2/g and pore sizes of 7 and 5 Å (Chang et al., 2019). In this case, the copper open metal sites are not exposed [150]. This disposition leads to two new types of micropores. The link distance of methane and nitrogen with these micropores is lower for methane, indicating a higher attraction. As previously, the Van der Waals forces ensure the selectivity; however, both the low specific surface area and the absence of open metal sites, lead to low methane adsorption capacities. In addition, ATC-Cu is synthetized by 1,3,5,7-adamantane tetracarboxylic acid as organic linker and copper as metallic ions. It possesses a BET specific surface area of 600 m^2/g and 0.23 cm^3/g of total pore volume. The arrangement of the atoms forms two cavities in which methane is adsorbed: 4.4 × 5.4 Å and 3.5 Å (Niu et al., 2019b). In this material, both attractive forces have an important role, since it has two zones for the adsorption of methane with very high adsorption enthalpies. In fact, selectivity and adsorption capacity are two of the highest of all the materials compiled. Other material is $Cu(INA)_2$, which consists of isonicotinic acid and metallic ions of copper. It presents a BET specific surface area of 251.8 m^2/g and a total pore volume of 0.12 cm^3/g. Its pores are rectangular channels of 4.7 Å (Hu et al., 2016). In this case, equal than for $Co_3(C_4O_4)_2(OH)_2$, Van der Waals forces have more importance, increasing the selectivity ratio. Finally, Kim et al. (2020) demonstrated that the incorporation of functional groups with high polarizability can enhance the methane uptake and the selectivity. It is the case of UiO-66, with the addition of Br_2. It presents a BET specific surface area of 622 m^2/g and a pore size between 7 and 8 Å. It presents a high desorption improvement in comparison with pristine UiO-66. This knowledge about the main characteristics in order to tailor the MOFs to improve methane separation was used by several authors to selectively separate methane from very diluted streams. For example, Chanajaree et al. (2019)) and Li et al. (2014c) have done Monte Carlo simulations for methane separation on ZIF MOFs. In case of a stream with 10% of methane in nitrogen at 298 K and atmospheric pressure, it was achieved a selectivity of 4.1 for the ZIF-78 MOF [157].

Concerning materials already described in methane storage section (Ni-MOF-74, Mg-MOF-74, MIL-100(Cr), HKUST-1 and MIL-100 V), the adsorption mechanisms are really similar, that is, the interaction between the adsorbate molecules and the open metal sites of the adsorbent (Li et al., 2014b). MOF-5 and MOF-177 adsorption is based mainly on its high BET specific surface area values in absence of open metal sites. Fig. 18 shows as the highest uptake capacities are for materials with open metal sites, whereas the highest selectivities are more related with pore size and the existence of specific zones for methane adsorption. Therefore, at low pressures, the pore size and the presence of both adsorptive forces (coulombic and Van der Waals) are more important than the BET specific surface area or total pore volume. Therefore, to achieve an efficient methane/nitrogen separation, materials must be designed with a pore size adjusted to the adsorbate, with the presence of not very strong open metal sites and with cavities in which Van der Waals forces are generated between the oxygen of the structure and the four hydrogens of the methane molecule.

Table 2
Properties of the different molecules present in a VAM stream (Lovas et al., 2004).

Compound	Molecular diameter (Å)	Dipole moment (D)	Polarizability ($Å^3$)
CH_4	3.82[a]	0	2.448
N_2	3.65[b]	0	1.710
CO_2	3.33[c]	0	2.507
O_2	3.47[b]	0	1.562
H_2O	2.80[d]	1.855	1.501

[a] Bao et al. (2011).
[b] Niwa et al. (1991).
[c] Anderson et al. (2012).
[d] Bunker (1994).

4. Effect of other components of the emissions on MOF adsorption properties

The comparison of the properties of the main VAM components, shows that all the molecules are non-polar, except water, and that carbon dioxide has the highest polarizability (Table 2). Concerning water, the presence of open metal sites hinders the performance of these materials in presence of moisture (Wang et al., 2019). Different works have obtained results that indicate that materials with high metallic valences (tri- or tetravalent metallic ions) are active water adsorbents (Inamdar et al., 2020). The polarity of the water molecule causes this attraction, enhancing the coverage of all the adsorption active sites, which hinders methane adsorption. In fact, Gonçalves et al. (Gonçalves et al., 2019) have studied the effect of the presence of water on the methane adsorption capacity of some of the most common MOFs (Cu-BTC, IRMOF-1, Mg-MOF-74, etc.), observing that the MOFs with open metal sites are the most affected by water. Cu-BTC presented a decrease of 2.2% in the total amount of methane adsorbed between pure methane and

Table 3
MOFs performance for selective adsorption.

Adsorbent	CH_4/N_2 selectivity	Uptake (mg CH_4/g)	Pressure (bar)	Temperature (K)	Reference
Al-CDC	13	20.96	1	298	Chang et al. (2020)
$CO_3(C_4O_4)_2(OH)_2$	12.5	5.92	1	298	Li et al. (2018b)
Cu-MOF	11	9.82	1	298	Chang et al. (2019)
ATC-Cu	9	44.8	1	298	Niu et al. (2019b)
$Cu(INA)_2$	8.3	13.23	1	298	Hu et al. (2016)
UiO-66-Br_2	5.1	11.52	1	298	Kim et al. (2020)
MOF-177	4	8.18	1	298	Saha et al. (2010)
Ni-MOF-74	3.8	22.75	1	298	Li et al. (2014b)
HKUST-1	3.7	13.15	1	298	Wang et al. (2002)
ZIF-8	3.1	5.2	1	196	Eyer et al. (2014)
MIL-100(Cr)	3	8.83	1	298	Li et al. (2014b)
MIL-100 V	3	3.57	1	298	Yang et al. (2015)
Ni-MOF-74	3	20.48	4	298	Li et al. (2014b)
Mg-MOF-74	1.5	24.27	1	298	Li et al. (2014b)
MOF-5	1.1	1.23	1	298	Saha et al. (2010)

methane with 140 ppm of water, whereas Mg-MOF-74 presented a decrease of 20% at the same conditions. On the other hand, materials without open metal sites do not present remarkable performance decreases. Likewise, the relative humidity influence was studied by demonstrated by Chidambaram et al. (2021). Accordingly, Rogacka et al. (2021) have made a screening of the best MOF materials for the separation of methane and carbon dioxide in presence of water. Some of the proposed MOFs are really hydrophilic, since the carbon dioxide adsorbed is displaced from open metal sites due to the presence of water. Most of the MOFs have been really affected by relative humidity over 30%. Likewise, García and Navalón (2018) have done a comprehensive compilation about the differences in adsorption depending on the moisture in the MOF structure. In order to avoid effectiveness losses, several authors have studied the different pathways to increase the hydrophobicity of the materials (Xie et al., 2020). Some of them have achieved good results, even largely retaining the original adsorptive properties of the materials. In spite of this, the techniques are not fully developed yet, so it would be recommended to perform a prior separation of moisture from the streams.

Concerning the other gases, the interaction strength on a polar adsorbent is $CO_2 > CH_4 > N_2 > O_2$ (Sui and Han, 2015). The higher polarizability of carbon dioxide than methane makes stronger the link with the open metal sites of the adsorbent (Li et al., 2020). In fact, carbon dioxide adsorption enthalpy is above 30 kJ/mol in some cases, which indicates an elevated bond strength (Lin et al., 2020). The same than in separation from nitrogen, some authors like Duan et al. (2018) have treated to enhance gas molecule-framework interaction by adjusting the cage size through changing the metal cluster, organic linker or synthesis conditions. In recent times, there are several manuscripts that deal with the CO_2/CH_4 separation (Awadallah and Al-Muhtaseb, 2021; Chen et al., 2020; Sheng et al., 2020; Mozafari et al., 2020). All the materials studied, including MOFs, presented higher affinity for carbon dioxide than for methane. The nonpolar covalent bonds in methane promote lower uptakes, due to the hydrophilic walls of these frameworks (Mohan et al., 2020). Hence, the importance carbon dioxide of preseparation from the stream, avoiding the poisoning of the adsorbent. It should also be noted that, in ventilation streams, the concentration of carbon dioxide is low, sometimes even at trace level.

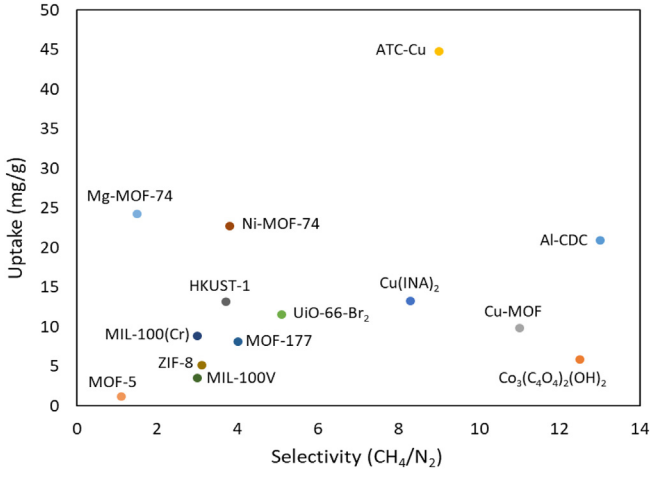

Fig. 18. Relation between methane uptake and CH_4/N_2 selectivity for different MOF materials.

5. Engineering aspects of the adsorption processes using MOFs

Concerning the packing of the solid adsorbent, conventional concentrators usually perform using fixed beds of granular adsorbents. In this way, the associated pressure drop leads to larger gas pumping costs. The pressure drop in a packed bed is usually described by the Ergun equation (Eq. (1).

$$\Delta P = \frac{150 \cdot \mu \cdot L}{{D_p}^2} \frac{(1-\varepsilon)^2}{\varepsilon^3} u_0 + \frac{1.75 \cdot L \cdot \rho}{D_p} \frac{(1-\varepsilon)}{\varepsilon^3} {u_0}^2 \quad (1)$$

where u_0 is the surface velocity, ρ and μ are the density and viscosity of the gas, respectively, D_p the particle diameter, L the length of the bed, and ε, the bed porosity. In a typical operation, for a surface velocity of 0.125 m/s and particle diameters of 162.5 and 520 μm, the pressure drop is of 172.5 and 53.7 Pa/m, respectively. This example illustrates the importance of the particle diameter both in the adsorption process and, hence, in energy consumption. Rezaei and Webley (2010) remarked that, in the case of structured adsorbents, monoliths or laminate structures ease suitable values of bed porosity (ε). In this way, Hong et al. (2015) proposed a MIL-101(Cr) monolith for carbon dioxide adsorption working at high pressure and low temperatures. Likewise, Rezaei et al. (2017) immobilized two MOFs, Ni-MOF-74 and UTSA-16 on commercial cordierite monolith for carbon dioxide capture, obtaining moderate adsorption capacities and fast kinetics. Several MOFs present high adsorption capacity losses after the shaping process, especially if these are modifications made by mechanical pressurization (Ursueguía et al., 2020). Therefore, the MOF shaping is a challenge for decreasing the pressure drop in concentrator units. These shaping processes should consider the relatively low thermal, chemical and mechanical stability of the materials, ensuring that adsorption properties of the material remain unaltered.

Concerning MOFs shaping, different approaches have been considered. Stable slurries formation, using organic binders such as polyvinyl alcohol aqueous solution, allows further material shaping by granulation or extrusion (Rubio-Martínez et al., 2017). Other approaches deal

with the milling of the MOF with a solid binder, such as graphite, followed by a pressure-driven pelletization of the mixture. In this case, the effect of the pelletizing pressure on the morphological properties of the MOFs must be considered. Finally, another possibility is the 3D printing technique. In fact, 3D-printed Ni-MOF-74 and UTSA-16 monoliths were tested for CO adsorption (Thakkar et al., 2017), with adsorption capacities of 1.35 and 1.31 mmol/g at 298 K, respectively, which represent the 79 and 87% of the capacities of their analogues MOF under the same conditions.

Another important issue, in order to achieve that MOFs will be used at large-scale applications, consists of its production. Since the first patent in 1995, MOFs production has progressed gradually, but a key point is the possibility of synthesizing these materials in large quantities with high efficiency. In this way, several efforts were made based on the solvent-free approach and water-based synthesis (Rubio-Martínez et al., 2017). However, add to the synthesis route, the downstream processing should be also improved, so large-scale application of MOFs will be limited by their commercial availability. Efforts in MOF commercialization have led to the creation of several spin off companies, such as MOF Apps, MOF Technologies and ProMOF. Likewise, among the MOF distributors, it is possible to find STREM Chemicals and Sigma Aldrich, the latter from BASF.

In summary, chemically suitable materials (adequate organic ligand and metal sites) are required, but without neglecting the engineering aspects. In this way, the ideal material would involve a low pressure drop design, resistant to humidity and high temperatures, and that could be manufactured on a large scale.

6. Conclusions and future recommendations

Methane separation from VAM streams by adsorption was discussed in this work. The features of these streams are: low methane concentration (<1%) in air, combined with high relative values of humidity and traces of carbon dioxide, at ambient temperature and pressure with high flowrates. With these conditions, MOFs are considered as an interesting choice for overcoming the limitations of the common adsorbents. In this review, a vast revision on the behaviour for methane storage at different pressures, and on different MOF structures was carried out. Pure methane adsorption in MOFs is mainly proportional to the specific surface area and pore volume at high pressures, whereas the presence of open metal sites (main contributors to Lewis acidity), as well as metal atoms density within the cavity, contribute to enhance the methane uptake at low pressures. Thus, structures like HKUST-1 and MOF-74 stand out for their methane storage capacity at atmospheric pressure, and also with ease of thermal regeneration.

The main challenge is the methane/nitrogen separation, for which combination of Van der Waals and coulombic forces are required. The first depends on the attraction between oxygen atoms of the adsorbent structure and the adsorbate molecules, being increased with a more tailored pore topology. The second effect depends on the presence of open metal sites in the structure. Likewise, an equilibrium between the number of open metal sites and their strength, which could lead to irreversible adsorption, is advisable. Materials presenting the best results are the ones specifically synthesized for this separation: (Al-CDC, $CO_3(C_4O_4)_2(OH)_2$, Cu-MOF and ATC-Cu).

The ideal material for the process must gather the features discussed above: high adsorption capacity (presence of a high concentration of open metal sites), hydrophobicity (low metallic oxidation states and as low as possible relative humidity conditions), easy regenerability by temperature increment and good methane selectivity values (high importance of Van der Waals forces).based on discussion here presented, future research studies should rely on these characteristics for the design of new materials applied to actual gas separation cases. In addition to the effectiveness of separation under ideal conditions, material stability at operation conditions should be also considered, thus shaping is a key point.

CRediT authorship contribution statement

David Ursueguía: Writing – original draft, Data curation, Writing – review & editing, Formal analysis. **Eva Díaz:** Writing – review & editing, Visualization, Conceptualization, Project administration. **Salvador Ordóñez:** Visualization, Conceptualization, Project administration, Supervision.

Declaration of competing interest

The authors declare that they have no known competing financial interests or personal relationships that could have appeared to influence the work reported in this paper.

Acknowledgments

This work was supported by the Research Fund for Coal and Steel of the European Union (contract 754077 - METHENERGY PLUS).

David Ursueguía acknowledges the Spanish Ministry of Education for the PhD grant that supports his research (FPU program).

References

Ahmadijokani, F., Ahmadipouya, S., Molavi, H., Rezakazemi, M., Aminabhavi, T., Arjmand, M., 2020. J. Environ. Manag. 274, 111155. https://doi.org/10.1016/j.jenvman.2020.111155.
Alezi, D., Belmabkhout, Y., Suyetin, M., Bhatt, P.M., Weseliński, L.J., Solovyeva, V., 2015. J. Am. Chem. Soc. 137, 13308–13318. https://doi.org/10.1021/jacs.5b07053.
Al-Jadir, T., Siperstein, F., 2018. Microporous Mesoporous Mater. 271, 160–168. https://doi.org/10.1016/j.micromeso.2018.06.002.
Alonso, A., Moral-Vico, J., Markeb, A. Abo, Busquets-Fité, M., Komilis, D., Puntes, V., 2017. Sci. Total Environ. 595, 51–62. https://doi.org/10.1016/j.scitotenv.2017.03.229.
Álvarez, M., Marín, P., Ordóñez, S., 2020. Mol. Catal. 487, 110886. https://doi.org/10.1016/j.mcat.2020.110886.
Anderson, M., Wang, H., Lin, Y.S., 2012. Rev. Chem. Eng. 28, 101–121. https://doi.org/10.1515/revce-2012-0001.
Awadallah, A., Al-Muhtaseb, S., 2021. Appl. Sci. 11, 265. https://doi.org/10.3390/app11010265.
Bao, Z., Alnemrat, S., Yu, L., Vasiliev, I., Ren, Q., Lu, X., Deng, S., 2011. J. Colloid Interface Sci. 357, 504–509. https://doi.org/10.1016/j.jcis.2011.01.103.
Baris, K., 2013. Energy Sustain. Dev. 17, 13–23. https://doi.org/10.1016/j.esd.2012.09.002.
Becker, T., Heinen, J., Dubbeldam, D., Lin, L., Vlugt, T., 2017. J. Phys. Chem. C 121, 4659–4673. https://doi.org/10.1021/acs.jpcc.6b12052.
Bon, V., 2017. Green Sus. Chem. 4, 44–49. https://doi.org/10.1016/j.chempr.2016.12.002.
Bonino, F., Chavan, S., Vitillo, J.G., Groppo, E., Agostini, G., Lamberti, C., 2008. Chem. Mater. 20, 4957–4968. https://doi.org/10.1021/cm800686k.
Borowski, M., Zyczkowski, P., Luczak, R., Karch, M., Cheng, J., 2020. Energies 13, 44. https://doi.org/10.3390/en13010044.
Bunker, B., 1994. J. Non-Crystalline Solids 179, 300–308. https://doi.org/10.1016/0022-3093(94)90708-0.
Cabello, C., Pozuelo, G., Opanasenko, M., Nachtigall, P., Čejka, J., 2016. ChemPlusChem 81, 828–835. https://doi.org/10.1002/cplu.201600168.
Carrott, P., Cansado, I., Carrott, M., 2006. Appl. Surf. Sci. 252, 5948–5952. https://doi.org/10.1016/j.apsusc.2005.11.014.
Cavenati, S., Grande, C.A., Rodrigues, A.E., 2004. J. Chem. Eng. Data 49, 1095–1101. https://doi.org/10.1021/je0498917.
Cavka, J., Jakobsen, S., Olsbye, U., Guillou, N., Lamberti, C., Bordiga, S., 2008. J. Am. Chem. Soc. 130, 13850–13851. https://doi.org/10.1021/ja8057953.
Chanajaree, R., Chokbunpiam, T., Kärger, J., Hannongbua, S., Fritzsche, S., 2019. Microporous Mesoporous Mater. 274, 266–276. https://doi.org/10.1016/j.micromeso.2018.07.023.
Chang, M., Zhao, Y., Yang, Q., Liu, D., 2019. ACS Omega 4, 14511–14516. https://doi.org/10.1021/acsomega.9b01740.
Chang, M., Zhao, Y., Liu, D., Yang, J., Li, J., Zhong, C., 2020. Sustainable Energy & Fuels 4, 138–142. https://doi.org/10.1039/C9SE00838A.
Chen, H., Fan, L., Zhang, X., Ma, L., 2020. ACS Appl. Nano Mater. 3, 2680–2686. https://doi.org/10.1021/acsanm.0c00041.
Chidambaram, A., Le, D., Navarro, J., Stylianou, K., 2021. Applied Mat. Today 22, 100933. https://doi.org/10.1016/j.apmt.2020.100933.
Chowdhury, P., Bikkina, C., Meister, D., Dreisbach, F., Gumma, S., 2009. Microporous Mesoporous Mater. 117, 406–413. https://doi.org/10.1016/j.micromeso.2008.07.029.
Cluff, D., Kennedy, G., Bennett, J., Foster, P., 2015. Appl. Therm. Eng. 90, 1151–1163. https://doi.org/10.1016/j.applthermaleng.2015.05.013.
Delgado, J., Uguina, M., Sotelo, J., Ruíz, B., Rosário, M., 2007. J. Nat. Gas Chem. 16, 235–243. https://doi.org/10.1016/S1003-9953(07)60054-1.
Bao, Z., Yu, L., Ren, Q., Lu, X., Deng, S., 2011. J. Colloid Interface Sci. 353, 549–556. https://doi.org/10.1016/j.jcis.2010.09.065.
Derwent, R., 2020. Atmosphere 11, 486. https://doi.org/10.3390/atmos11050486.
Dhakshinamoorthy, A., Alvaro, M., Horcajada, P., Gibson, E., Vishnuvarthan, M., Vimont, A., 2012. ACS Catal. 2, 2060–2065. https://doi.org/10.1021/cs300345b.

Díaz, E., Fernández, J., Ordóñez, S., Canto, N., González, A., 2012. Ecol. Indic. 18, 126–130. https://doi.org/10.1016/j.ecolind.2011.11.009.
Dietzel, P., Besikiotis, V., Blom, R., 2009. J. Mater. Chem. 19, 7362–7370. https://doi.org/10.1039/b911242a.
Duan, X., Yu, B., Lv, R., Ji, Z., Li, B., Cui, Y., 2018. Polyhedron 155, 332–336. https://doi.org/10.1016/j.poly.2018.08.056.
Düren, T., Sarkisov, L., Yaghi, O., Snurr, R., 2004. Langmuir 20, 2683–2689. https://doi.org/10.1021/la0355500.
Embrechts, H., Kriesten, M., Ermer, M., Peukert, W., Hartmann, M., Distaso, M., 2020. RSC Adv. 10, 7336–7348. https://doi.org/10.1039/C9RA09968A.
Erdogan, S., Karacan, O., Okandan, E., 2014. Int. J. Rock Mech. Min. Sci. 63, 148–158. https://doi.org/10.1016/j.ijrmms.2013.08.008.
Esteves, I., Lopes, M., Nunes, P., Mota, J., 2008. Sep. Purif. Technol. 62, 281–296. https://doi.org/10.1016/j.seppur.2008.01.027.
Eyer, S., Stadie, N., Borgschulte, A., Emmenegger, L., Mohn, J., 2014. Adsorption 20, 5–6. https://doi.org/10.1007/s10450-014-9609-9.
Farha, O., Wilmer, C., Eryazici, I., Hauser, B., Parilla, P., O'Neill, K., 2012. J. Am. Chem. Soc. 134, 9860–9863. https://doi.org/10.1021/ja302623w.
Fernández, J., Marín, P., Díez, F., Ordóñez, S., 2016. App. Thermal Eng. 102, 167–175. https://doi.org/10.1016/j.applthermaleng.2016.03.171.
Furukawa, H., Ko, N., Go, Y., Aratani, N., Choi, S., Choi, E., Özgür, A., Snurr, R., O'Keeffe, M., Kim, J., Yaghi, O., 2010. Science 23, 424–428. https://doi.org/10.1126/science.1192160.
Gao, J., Guan, C., Zhang, B., 2020. Sci. Total Environ. 725, 138295. https://doi.org/10.1016/j.scitotenv.2020.138295.
García, A., Vallone, A., Korili, S., Gil, A., Sapag, K., 2016. Microporous Mesoporous Mater. 224, 323–331. https://doi.org/10.1016/j.micromeso.2016.01.002.
García, H., Navalón, S., 2018. Metal-Organic Frameworks: Applications in Separations and Catalysis. first ed. John Wiley & Sons https://doi.org/10.1002/9783527809097.ch5.
Gedrich, K., Senkovska, I., Klein, N., Stoeck, U., Henschel, A., Martin, R. Lohe, 2010. Angew. Chem. 49, 8489–8492. https://doi.org/10.1002/anie.201001735.
Ghanbari, T., Abnisa, F., Daud, W., 2020. Sci. Total Environ. 707, 135090. https://doi.org/10.1016/j.scitotenv.2019.135090.
Ghazvini, M., Vahedi, M., Nobar, S., Sabouri, F., 2021. J. Environ. Chem. Eng. 9, 104790. https://doi.org/10.1016/j.jece.2020.104790.
Gholipour, F., Mofarahi, M., 2016. J. Supercrit. Fluids 111, 47–54. https://doi.org/10.1016/j.supflu.2016.01.008.
Ghoshal, A., Manjare, S., Loss, J., 2002. Prev. Process Ind. 15, 413–421. https://doi.org/10.1016/S0950-4230(02)00042-6.
Glover, T., Peterson, G., Schindler, B., Britt, D., Yaghi, O., 2011. Chem. Eng. Sci. 66, 163–170. https://doi.org/10.1016/j.ces.2010.10.002.
Gonçalves, D., Snurr, R., Lucena, S., 2019. Adsorption 25, 1633–1642. https://doi.org/10.1007/s10450-019-00165-8.
Goraya, N., Rajpoot, N., Sivagnanam, B., 2019. ChemistrySelect 4, 3585–3601. https://doi.org/10.1002/slct.201803633.
Guo, Z., Wu, H., Srinivas, G., Zhou, Y., Xiang, S., Chen, Z., 2011. Angew. Chem. 50, 3178–3181. https://doi.org/10.1002/anie.201007583.
Hamon, L., Jolimaître, E., Pirngruber, G.D., 2010. Ind. Eng. Chem. Res. 49, 7497–7503. https://doi.org/10.1021/ie902008g.
He, Y., Li, B., O'keeffe, M., Chen, B., 2014. Chem. Soc. Rev. 43, 5618–5656. https://doi.org/10.1039/C4CS00041B.
Henni, A., Tontiwachwuthikul, P., Chakma, A., 2006. J. Chem. Eng. Data 51, 64–67. https://doi.org/10.1021/je050172h.
Hong, D., Hwang, Y., Serre, C., Ferey, G., Chang, J., 2009. Adv. Funct. Mater. 19, 1537–1552. https://doi.org/10.1002/adfm.200801130.
Hong, W., Perera, S., Burrows, A., 2015. Microporous Mesoporous Mater. 214, 149–155. https://doi.org/10.1016/j.micromeso.2015.05.014.
Hou, X., Liu, S., Zhu, Y., Yang, Y., 2020. Fuel 268, 117349. https://doi.org/10.1016/j.fuel.2020.117349.
Hu, J., Sun, T., Liu, X., Guo, Y., Wang, S., 2016. RSC Adv. 6, 64039–64046. https://doi.org/10.1039/C6RA12280A.
Hwang, Y., Hong, D., Chang, J., Jhung, S., Seo, Y., Kim, J., 2008. Angew. Chem. 120, 4212–4216. https://doi.org/10.1002/anie.200705998.
Inamdar, A., Pathak, A., Usman, M., Chiou, K., Tsai, P., Mendiratta, S., Kamal, S., Liu, Y., Chen, J., Chiang, M., Lu, K., 2020. J. Mater. Chem. A 8, 11958–11965. https://doi.org/10.1039/D0TA00605J.
Javani, R., Maghsoudi, H., Gilan, S., Majidpour, M., 2020. Sep. Sci. Technol., 1–16 https://doi.org/10.1080/01496395.2020.1842889.
Kacem, M., Pellerano, M., Delebarre, A., 2015. Fuel Process. Technol. 138, 271–283. https://doi.org/10.1016/j.fuproc.2015.04.032.
Karakurt, I., Aydin, G., Aydiner, K., 2011. Renew. Sust. Energ. Rev. 15, 1042–1049. https://doi.org/10.1016/j.rser.2010.11.030.
Katz, M., Brown, Z., Colón, Y., Siu, P., Scheidt, K., Snurr, R., 2013. Chem. Commun. 49, 9449–9451. https://doi.org/10.1039/C3CC46105J.
Kaye, S., Dailly, A., Yaghi, O., Long, J., 2007. J. Am. Chem. Soc. 129, 14176–14177. https://doi.org/10.1021/ja076877g.
Kim, J., Maiti, A., Lin, L., Stolaroff, J., Smit, B., Aines, R., 2013. Nat. Commun. 4, 1–7. https://doi.org/10.1038/ncomms2697.
Kim, T., Kim, S., Yoon, T., Kim, M., Park, W., Han, H., Kong, C., Park, C., Kim, J., Bae, Y., 2020. Chem. Eng. J. 399, 125717. https://doi.org/10.1016/j.cej.2020.125717.
Kizzie, A., Dailly, A., Perry, L., Lail, M., Lu, W., Nelson, T., 2014. Mater. Sci. Appl. 5, 387. https://doi.org/10.4236/msa.2014.56044.
Knyazena, M., Tsivadze, A., Solovtsova, O., Fomkin, A., Pribylov, A., Shkolin, A., Pulin, A., Menshchikov, I., 2019. Physicochem. Process. Interfaces 55, 9–14. https://doi.org/10.1134/S2070205119010064.
Koc, R., Kazantzis, N., Nuttall, W., Ma, Y., 2013. J. Loss Prev. Process Ind. 26, 468–477. https://doi.org/10.1016/j.jlp.2012.07.012.
Kokçam, U., Goldman, A., Esrafili, L., Gharib, M., Morsali, A., Weingart, O., Janiak, C., 2020. Chem. Soc. Rev. 49, 2751–2798. https://doi.org/10.1039/c9cs00609e.
Krause, S., Bon, V., Senkovska, I., Többens, D.M., Wallacher, D., Pillai, R.S., 2018. Nat. Commun. 9, 1573. https://doi.org/10.1038/s41467-018-03979-2.
Lázaro, I., Wells, C., Forgan, R., 2020. Angew. Chem. Int. Edit. 59, 5211–5217. https://doi.org/10.1002/anie.201915848.
Lee, J., Jhung, S., Yoon, J., Hwang, Y., Chang, J., 2009. J. Ind. Eng. Chem. 15, 674–676. https://doi.org/10.1016/j.jiec.2009.09.043.
Li, B., Wen, H., Wang, H., Wu, H., Tyagi, M., Yildirim, T., Zhou, W., Chen, B., 2014a. J. Am. Chem. Soc. 136, 6207–6210. https://doi.org/10.1021/ja501810r.
Li, B., Wen, H., Zhou, W., Jeff, Q. Xu, Chen, B., 2016a. Chem. 1, 557–580. https://doi.org/10.1016/j.chempr.2016.09.009.
Li, B., Wen, H., Zhou, W., Xu, J., Chen, B., 2016b. Chem 1, 557–580. https://doi.org/10.1016/j.chempr.2016.09.009.
Li, H., Wang, K., Sun, Y., Lollar, C., Li, J., Zhou, H., 2018a. Mater. Today 21, 108–121. https://doi.org/10.1016/j.mattod.2017.07.006.
Li, J., Kuppler, R., Zhou, H., 2009. Chem. Soc. Rev. 38, 1477–1504. https://doi.org/10.1039/B802426J.
Li, L., Yang, J., Li, J., Chen, Y., Li, J., 2014b. Microporous Mesoporous Mater. 198, 236–246. https://doi.org/10.1016/j.micromeso.2014.07.041.
Li, L., Yang, L., Wang, J., Zhang, Z., Yang, Q., Yang, Y., Ren, Q., Bao, Z., 2018b. AICHE J. 64, 3681–3689. https://doi.org/10.1002/aic.16335.
Li, Z., Xiao, G., Yang, Q., Xiao, Y., Zhong, C., 2014c. Chem. Eng. Sci. 120, 59–66. https://doi.org/10.1016/j.ces.2014.08.003.
Li, Z., Wu, Z., Qin, Z., Zhu, H., Wu, J., Wang, R., Lei, L., Chen, J., Dong, M., Fan, W., Wang, J., 2017. Fuel Process. Technol. 160, 102–108. https://doi.org/10.1016/j.fuproc.2017.02.030.
Li, Z., Liu, P., Ou, C., Dong, X., 2020. ACS Sustain. Chem. Eng. 8, 15378–15404. https://doi.org/10.1021/acssuschemeng.0c05155.
Lin, J., He, C., Liu, Y., Liao, P., Zhou, D., Zhang, J., Chen, X., 2016. Angew. Chem. Int. 55, 4674–4678. https://doi.org/10.1002/anie.201511006.
Lin, R., Li, L., Alsalme, A., Chen, B., 2020. Small Structures 1, 2000022. https://doi.org/10.1002/sstr.202000022.
Lin, Y., Kong, C., Zhang, Q., Chen, L., 2017. Adv. Energy Mater. 7, 1601296. https://doi.org/10.1002/aenm.201601296.
Liu, Q., Ning, L., Zheng, S., Tao, M., Shi, Y., He, Y., 2013. Sci. Rep. 3, 2916. https://doi.org/10.1038/srep02916.
Liu, Y., Liu, D., Yang, Q., Zhong, C., Mi, J., 2010. Ind. Eng. Chem. Res. 49, 2902–2906. https://doi.org/10.1021/ie901488f.
Llewellyn, P., Bourrelly, S., Serre, C., Vimont, A., Daturi, M., Hamon, L., 2008. Langmuir 24, 7245–7250. https://doi.org/10.1021/la800227x.
Lokhandwala, K., Pinnau, I., He, Z., Amo, K., DaCosta, A., Wijmans, J., Baker, R., 2010. J. Membr. Sci. 346, 270–279. https://doi.org/10.1016/j.memsci.2009.09.046.
Lovas, F., Suenram, R., Coursey, J., Kotochigova, S., Chang, J., Olsen, K., Dragoset, R., 2004. NIST Standard Reference Database. 115. https://doi.org/10.18434/T4PC70.
Lu, W., Yuan, D., Zhao, D., Schilling, C., Plietzsch, O., Muller, T., 2010. Chem. Mater. 22, 5964–5972. https://doi.org/10.1021/cm1021068.
Lu, Z., Du, L., Tang, K., Bai, J., 2013. Cryst. Growth Des. 13, 2252–2255. https://doi.org/10.1021/cg400449c.
Lucena, S., Mileo, P., Silvino, P., Cavalcante, C., 2011. J. Am. Chem. Soc. 133, 19282–19285. https://doi.org/10.1021/ja207593c.
Ma, S., Zhou, H.-C., 2010. Chem. Commun. 46, 44–53. https://doi.org/10.1039/B916295J.
Ma, S., Sun, D., Simmons, J., Collier, C., Yuan, D., Zhou, H., 2008. J. Am. Chem. Soc. 130, 1012–1016. https://doi.org/10.1021/ja0771639.
Masala, A., Vitillo, J.G., Bonino, F., Manzoli, M., Grande, C.A., Bordiga, S., 2016. Phys. Chem. Chem. Phys. 18, 220–227. https://doi.org/10.1039/C5CP05905D.
Mason, J., Veenstra, M., Long, J., 2014. Chem. Sci. 5, 32–51. https://doi.org/10.1039/C3SC52633J.
Mason, J.A., Oktawiec, J., Taylor, M.K., Hudson, M.R., Rodriguez, J., Bachman, J.E., 2015. Nature 527, 357–361. https://doi.org/10.1038/nature15732.
Mi, B., 2019. Science 364, 1033–1034. https://doi.org/10.1126/science.aax3103.
Mohan, M., Essalhi, M., Durette, D., Rana, L., Ayevide, F., Maris, T., Duong, A., 2020. ACS Appl. Mater. Interfaces 12, 50619–50627. https://doi.org/10.1021/acsami.0c15395.
Mozafari, M., Rahimpour, A., Abedini, R., 2020. J. Ind. Eng. Chem. 85, 102–110. https://doi.org/10.1016/j.jiec.2020.01.030.
Niu, R., Liu, P., Li, W., Wang, S., Li, J., 2019a. Microporous Mesoporous Mater. 284, 235–240. https://doi.org/10.1016/j.micromeso.2019.04.044.
Niu, Z., Cui, X., Pham, T., Lan, P., Xing, H., Forrest, K., Wojtas, L., Space, B., Ma, S., 2019b. Angew. Chem. Int. Edit. 58, 10138–10141. https://doi.org/10.1002/anie.201904507.
Niwa, M., Yamazaki, K., Murakami, Y., 1991. Ind. Eng. Chem. Res. 30, 38–42. https://doi.org/10.1021/ie00049a006.
Nosike, E., Jiang, Z., Miao, L., Akakuru, O., Yuan, B., Wu, S., Zhang, Y., Zhang, Y., Wu, A., 2020. J. Hazard. Mater. 392, 122288. https://doi.org/10.1016/j.jhazmat.2020.122288.
Oboirien, B., North, B., Obayopo, S., Odusote, J., Sadiku, E., 2018. Energy Stra. Rev. 20, 64–70. https://doi.org/10.1016/j.esr.2018.01.002.
Øien-Ødegaard, S., Bouchevreau, B., Hylland, K., Wu, L., Blom, R., Grande, C., 2016. Inorg. Chem. 55, 1986–1991. https://doi.org/10.1021/acs.inorgchem.5b02257.
Park, K., Ni, Z., Côté, A., Choi, J., Huang, R., Uribe-Romo, F., Chae, H., O'Keeffe, M., Yaghi, O., 2006. PNAS 103, 10186–10191. https://doi.org/10.1073/pnas.0602439103.
Pavloudakis, F., Roumpos, C., Karlopoulos, E., Koukouzas, N., 2020. Energies 13, 3995. https://doi.org/10.3390/en13153995.
Peng, Y., Krungleviciute, V., Eryazici, I., Hupp, J.T., Farha, O.K., Yildirim, T., 2013. J. Am. Chem. Soc. 135, 11887–11894. https://doi.org/10.1021/ja4045289.

Pham, T., Forrest, K., Space, B., 2016. Phys. Chem. Chem. Phys. 18, 21421–21430. https://doi.org/10.1039/C6CP02650H.
Phuong, V., Chokbunpiam, T., Fritzsche, S., Remsungnen, T., Rungrotmongkol, T., Chmelik, C., 2016. Microporous Mesoporous Mater. 235, 69–77. https://doi.org/10.1016/j.micromeso.2016.06.029.
Polyukhov, D., Krause, S., Bon, V., Poryvaev, A., Kaskel, S., Fedin, M., 2020. J. Phys. Chem. Lett. 11, 5856–5862. https://doi.org/10.1021/acs.jpclett.0c01705.
Qin, B., Li, L., Ma, D., Lu, Y., Zhong, X., Jia, Y., 2016. PSEP 103, 203–211. https://doi.org/10.1016/j.psep.2016.07.005.
Rahmani, A., Emrooz, H., Abedi, S., Morsali, A., 2018. Mater. Sci. Semicond. Process. 80, 44–51. https://doi.org/10.1016/j.mssp.2018.02.013.
Ramos-Fernández, E., 2014. Boletín del Grupo Español del Carbón. 32 pp. 19–25.
Ramsahye, N., Trens, P., Shepherd, C., Gonzalez, P., Trung, T., Ragon, F., 2014. Microporous Mesoporous Mater. 189, 222–231. https://doi.org/10.1016/j.micromeso.2013.09.005.
Rao, X., Cai, J., Yu, J., He, Y., Wu, C., Zhou, W., 2013. Chem. Commun. 49, 6719–6721. https://doi.org/10.1039/C2TA00155A.
Rezaei, F., Webley, P., 2010. Sep. Purif. Technol. 70, 243–256. https://doi.org/10.1016/j.seppur.2009.10.004.
Rezaei, F., Lawson, S., Hosseini, H., Thakkar, H., Hajari, A., Monjezi, S., Rownaghi, A., 2017. Chem. Eng. J. 313, 1346–1353. https://doi.org/10.1016/j.cej.2016.11.058.
Rogacka, J., Seremak, A., Luna-Triguero, A., Formalik, F., Matito-Martos, I., Firlej, L., Calero, S., Kuchta, B., 2021. Chem. Eng. J. 403, 126392. https://doi.org/10.1016/j.cej.2020.126392.
Rother, J., Fieback, T., 2013. Adsorption 19, 1065–1074. https://doi.org/10.1007/s10450-013-9527-2.
Rubio-Martínez, M., Avci-Camur, C., Thornton, A., Imaz, I., Maspoch, D., Hill, M., 2017. Chem. Soc. Rew. 46, 3453–3480. https://doi.org/10.1039/C7CS00109F.
Saha, D., Deng, S., 2010a. J. Phys. Chem. Lett. 1, 73–78. https://doi.org/10.1021/jz900028u.
Saha, D., Deng, S., 2010b. Tsinghua SciTechnol. 15, 363–376. https://doi.org/10.1016/S1007-0214(10)70075-4.
Saha, D., Bao, Z., Jia, F., Deng, S., 2010. Environ. Sci. Technol. 44, 1820–1826. https://doi.org/10.1021/es9032309.
Sahoo, B., 2016. Synthesis and characterizations of novel Metal-Organic Frameworks (MOFs). Visible Light Photocatalyzed Redox-Neutral Organic Reactions and Synthesis of Novel Metal-Organic Frameworks. Springer https://doi.org/10.1007/978-3-319-48350-4_5.
Saleman, T., Li, G., Rufford, T., Stanwix, P., Chan, K., Huang, S., May, E., 2015. Chem. Eng. J. 281, 739–748. https://doi.org/10.1016/j.cej.2015.07.001.
Senkovska, I., Kaskel, S., 2008. Microporous Mesoporous Mater. 112, 108–115. https://doi.org/10.1016/j.micromeso.2007.09.016.
Shah, K., Moghtaderi, B., Doroodchi, E., Sandford, J., 2015. Fuel Process. Technol. 140, 285–296. https://doi.org/10.1016/j.fuproc.2015.07.031.
Sheng, L., Guo, Y., Zhao, D., Ren, J., Wang, S., Deng, M., 2020. J. Nat. Gas Sci. Eng. 75, 103123. https://doi.org/10.1016/j.jngse.2019.103123.
Singh, A., Kumar, J., 2016. Energy Procedia 90, 336–348. https://doi.org/10.1016/j.egypro.2016.11.201.
Spanopoulos, I., Tsangarakis, C., Klontzas, E., Tylianakis, E., Froudakis, G., Adil, K., 2016. J. Am. Chem. Soc. 138, 1568–1574. https://doi.org/10.1021/jacs.5b11079.
Sridhar, P., Kaisare, N., 2020. J. Ind. Eng. Chem. 85, 170–180. https://doi.org/10.1016/j.jiec.2020.01.038.
Stoeck, U., Krause, S., Bon, V., Senkovska, I., Kaskel, S., 2012. Chem. Commun. 48, 10841–10843. https://doi.org/10.1039/C2CC34840C.
Su, S., Beath, A., Guo, H., Mallett, C., 2005. Prog. Energy Combust. Sci. 31, 123–170. https://doi.org/10.1016/j.pecs.2004.11.001.
Su, S., Chen, H., Teakle, P., Xue, S., 2008. J. Environ. Manag. 86, 44–62. https://doi.org/10.1016/j.jenvman.2006.11.025.
Sui, Z., Han, B., 2015. Carbon 82, 590–598. https://doi.org/10.1016/j.carbon.2014.11.014.
Sun, B., Kayal, S., Chakraborty, A., 2014. Energy 76, 419–427. https://doi.org/10.1016/j.energy.2014.08.033.
Sun, D., Ma, S., Simmons, J., Li, J., Yuan, D., Zhou, H., 2010. Chem. Commun. 46, 1329–1331. https://doi.org/10.1039/b920995f.
Szczęśniak, B., Choma, J., Jaroniec, M., 2018. J. Colloid Interface. Sci. 514, 801–813. https://doi.org/10.1016/j.jcis.2017.11.049.
Szlazak, N., Obracaj, D., Swolkien, J., 2020. Mining Metall. Explor. 37, 567–579. https://doi.org/10.1007/s42461-020-00190-0.
Tagliabue, M., Farrusseng, D., Valencia, S., Aguado, S., Ravon, U., Rizzo, C., 2009. Chem. Eng. J. 155, 553–566. https://doi.org/10.1016/j.cej.2009.09.010.
Tahmooresi, M., Sabzi, F., 2014. Fluid Ph. Equilibria. 381, 83–89. https://doi.org/10.1016/j.fluid.2014.08.020.
Tan, F., Liu, M., Li, K., Wang, Y., Wang, J., Guo, X., 2015. Chem. Eng. J. 281, 360–367. https://doi.org/10.1016/j.cej.2015.06.044.
Thakkar, H., Eastman, S., Al-Naddaf, Q., Rownaghi, A., Rezaei, F., 2017. Appl. Mater. Interfaces 9, 35908–35916. https://doi.org/10.1021/acsami.7b11626.
Triebe, R., Tezel, F., Khulbe, K., 1996. Gas Sep. Pur. 10, 81–84. https://doi.org/10.1016/0950-4214(95)00016-X.
Ursueguía, D., Díaz, E., Ordóñez, S., 2020. Nanomaterials 10, 1089. https://doi.org/10.3390/nano10061089.
Valvekens, P., Vandichel, M., Waroquier, M., Speybroeck, V. Van, Vos, D. De, 2014. J. Catal. 317, 1–10. https://doi.org/10.1016/j.jcat.2014.06.006.
Vandenbrande, S., Verstraelen, T., Gutiérrez-Sevillano, J.J., Waroquier, M., van Speybroeck, V., 2017. J. Phys. Chem. C 121, 25309–25322. https://doi.org/10.1021/acs.jpcc.7b08971.
Wang, B., Liu, J., Yu, J., Lv, J., Dong, C., Li, J., 2020. J. Hazard. Mater. 382, 121018. https://doi.org/10.1016/j.jhazmat.2019.121018.
Wang, C., Luo, Y., He, X., Hong, D., Wang, J., Chen, F., Chen, C., Sun, B., 2019. Inorg. Chem. 58, 3058–3064. https://doi.org/10.1021/acs.inorgchem.8b03042.
Wang, L., Deng, H., Furukawa, H., Gándara, F., Cordova, K., Peri, D., 2014. Inorg. Chem. 53, 5881–5883. https://doi.org/10.1021/ic500434a.
Wang, Q., Shen, D., Büllow, M., Lau, M., Deng, S., Fitch, F., Lemcoff, N., Semanscin, J., 2002. Microporous Mesoporous Mater. 55, 217–230. https://doi.org/10.1016/S1387-1811(02)00405-5.
Wang, Y., Yang, R., 2019. ACS Sustain. Chem. Eng. 7, 3301–3308. https://doi.org/10.1021/acssuschemeng.8b05339.
Wiersum, A., Chang, J., Serre, C., Llewellyn, P., 2013. Langmuir 29, 3301–3309. https://doi.org/10.1021/la3044329.
Wilmer, C., Farha, O., Yildirim, T., Eryazici, I., Krungleviciute, V., Sarjeant, A., Snurr, R., Hupp, J., 2013. Energy Environ. Sci. 6, 1158–1163. https://doi.org/10.1039/C3EE24506C.
Wong-Foy, A., Matzger, A., Yaghi, O., 2006. J. Am. Chem. Soc. 128, 3494–3495. https://doi.org/10.1021/ja058213h.
Wu, D., Guo, X., Sun, H., Navrotsky, A., 2015. J. Phys. Chem. Lett. 6, 2439–2443. https://doi.org/10.1021/acs.jpclett.5b00893.
Wu, H., Zhou, W., Yildirim, T., 2009. J. Am. Chem. Soc. 131, 4995–5000. https://doi.org/10.1021/ja900258t.
Wu, H., Simmons, J., Liu, Y., Brown, C., Wang, X., Ma, S., Peterson, V., Southon, P., Kepert, C., Zhou, H., Yildirim, T., Zhou, W., 2010. Chem. Eur. J. 16, 5205–5214. https://doi.org/10.1002/chem.200902719.
Wu, X., Yuan, B., Bao, Z., Deng, S., 2014. J. Colloid Interface Sci. 430, 78–84. https://doi.org/10.1016/j.jcis.2014.05.021.
Xie, L., Xu, M., Liu, X., Zhao, M., Li, J., 2020. Adv. Sci. 7, 1901758. https://doi.org/10.1002/advs.201901758.
Xie, S., Lin, S., Zhang, Q., Tian, Z., Wang, Y., 2018. J. Energy Chem. 27, 1629–1636. https://doi.org/10.1016/j.jechem.2018.03.015.
Xiong, R., Odbadrakh, K., Michalkova, A., Luna, J.P., Petrova, T., Keffer, D.J., 2010. Sensors Actuators B Chem. 148, 459–468. https://doi.org/10.1016/j.snb.2010.05.064.
Yang, J., Wang, Y., Li, L., Zhang, Z., Li, J., 2015. J. Colloid Interface Sci. 456, 197–205. https://doi.org/10.1016/j.jcis.2015.06.036.
Yang, L., Ravindran, P., Vajeeston, P., Tilset, M., 2012. Phys. Chem. Chem. Phys. 14, 4713–4723. https://doi.org/10.1039/C2CP24091B.
Yang, R., 2003. Adsorbents: Fundamentals and Applications. first ed. John Wiley & Sons https://doi.org/10.1002/047144409X.
Yi, H., Li, F., Ning, P., Tang, X., Peng, J., Li, Y., 2013. Chem. Eng. J. 215–216, 635–642. https://doi.org/10.1016/j.cej.2012.11.050.
Yin, J., Su, S., Yu, X., Bae, J., Jin, Y., Villella, A., Jara, M., Ashby, M., Cunnington, M., Loney, M., 2020. Energy Fuel 34, 9885–9893. https://doi.org/10.1021/acs.energyfuels.0c01681.
Yuan, D., Zheng, Y., Li, Q., Lin, B., Zhang, G., Liu, J., 2018. Powder Technol. 333, 377–384. https://doi.org/10.1016/j.powtec.2018.04.045.
Zhang, X., Xiao, P., Chen, G., Sun, C., Yang, L., 2018. Chem. Eng. Technol. 41, 1818–1825. https://doi.org/10.1002/ceat.201700402.
Zhang, X., Chen, Z., Liu, X., Hanna, S., Wang, X., Taheri-Ledari, R., Maleki, A., Li, P., Farha, O., 2020. Chem. Soc. Rev. 49, 7406–7427. https://doi.org/10.1039/D0CS00997K.
Zhao, T., Jeremias, F., Boldog, I., Nguyen, B., Henninger, S.K., Janiak, C., 2015. Dalton Trans. 44, 16791–16801. https://doi.org/10.1039/C5DT02625C.
Zheng, B., Liu, Y., Liu, R., Meng, J., 2015. Int. J. Hydrog. Energy 40, 3381–3387. https://doi.org/10.1016/j.ijhydene.2015.01.020.
Zheng, Y., Li, Q., Yuan, C., Tao, Q., Zhao, Y., Zhang, G., Liu, J., 2019. Powder Technol. 347, 42–49. https://doi.org/10.1016/j.powtec.2019.02.042.
Zhou, W., 2010. Chem. Rec. 10, 200–204. https://doi.org/10.1002/tcr.201000004.